



1 **Connecting the Greenland ice-core and U/Th timescales**
2 **via cosmogenic radionuclides: Testing the synchronicity of**
3 **Dansgaard-Oeschger events**

4 Florian Adolphi^{1,2}, Christopher Bronk Ramsey³, Tobias Erhardt¹, R. Lawrence Edwards⁴, Hai
5 Cheng^{4,5}, Chris S. M. Turney⁶, Alan Cooper⁷, Anders Svensson⁸, Sune O. Rasmussen⁸,
6 Hubertus Fischer¹ and Raimund Muscheler²

7 ¹Climate and Environmental Physics, Physics Institute & Oeschger Centre for Climate Change Research,
8 University of Bern, Sidlerstrasse 5, 3012 Bern, Switzerland

9 ²Quaternary Sciences, Department of Geology, Lund University, Sölvegatan 12, 22362 Lund, Sweden

10 ³Research Laboratory for Archaeology and the History of Art, University of Oxford, Dyson Perrins Building,
11 South Parks Road, Oxford OX1 3QY, UK

12 ⁴Institute of Global Environmental Change, Xi'an Jiatong University, Xi'an 710049, China

13 ⁵Department of Earth Sciences, University of Minnesota, Minneapolis, Minnesota, 55455, USA

14 ⁶Palaeontology, Geobiology and Earth Archives Research Centre and ARC Centre of Excellence in Australian
15 Biodiversity and Heritage, School of Biological, Earth and Environmental Sciences, University of New South
16 Wales, Sydney, NSW 2052, Australia

17 ⁷Australian Centre for Ancient DNA and ARC Centre of Excellence in Australian Biodiversity and Heritage,
18 School of Biological Sciences, The University of Adelaide, Adelaide, SA 5005, Australia

19 ⁸Centre for Ice and Climate, Niels Bohr Institute, University of Copenhagen, Juliane Maries Vej 30, 2100
20 Copenhagen, Denmark

21 *Correspondence to:* Florian Adolphi (adolphi@climate.unibe.ch)

22 **Abstract.** During the last glacial period Northern Hemisphere climate was characterized by extreme and abrupt
23 climate changes, so-called Dansgaard-Oeschger (DO) events. Most clearly observed as temperature changes in
24 Greenland ice-core records, their climatic imprint was geographically widespread. However, the temporal
25 relation between DO-events in Greenland and other regions is uncertain due to the chronological uncertainties of
26 each archive, limiting our ability to test hypotheses of synchronous change. On the contrary, the assumption of
27 direct synchrony of climate changes forms the basis of many timescales. Here, we use cosmogenic radionuclides
28 (¹⁰Be, ³⁶Cl, ¹⁴C) to link Greenland ice-core records to U/Th-dated speleothems, quantify offsets between both
29 timescales, and improve their absolute dating back to 45,000 years ago. This approach allows us to test the
30 assumption that DO-events occurred synchronously between Greenland ice-core and tropical speleothem
31 records at unprecedented precision. We find that the onset of DO-events occurs within synchronization
32 uncertainties in all investigated records. Importantly, we demonstrate that there remain local discrepancies in the
33 temporal development of rapid climate change for specific events and speleothems. These may be either related
34 to the location of proxy records relative to the shifting atmospheric fronts or to underestimated U/Th-dating
35 uncertainties. Our study thus highlights the potential for misleading interpretations of the Earth system when
36 applying the common practice of climate wiggle-matching.

37 **1 Introduction**

38 Precise and accurate chronologies are critical for understanding past environmental and climatic changes.

39 Global natural and anthropogenic archives can only be directly compared through the development of robust



40 chronological frameworks, enabling studies of the spatiotemporal dynamics of past change. These findings are
41 crucial for understanding the nature and cause of rapid climate changes in the past, and hence, characterizing the
42 dynamics and feedbacks of past and projected future climate change (Thomas, 2016). However, the
43 applicability, precision, and accuracy of the available dating methods pose strong constraints on our ability to
44 infer leads and lags between climate records, and ultimately, mechanisms of change in the Earth system.
45 Instead, the situation is often reversed: climate changes such as Dansgaard-Oeschger, or DO, events (Dansgaard
46 et al., 1993; Dansgaard et al., 1969) are typically *assumed* to occur synchronously across the Northern
47 Hemisphere in different climate proxies from various regions and then used as chronological tie-points. This so-
48 called “climate wiggle-matching” forms the chronological basis of a large part of paleoclimate records (e.g.,
49 Bard et al., 2013; Hughen et al., 2006; Henry et al., 2016; Turney et al., 2015), especially in the marine realm
50 where other dating methods suffer from low precision and poorly constrained biases such as the marine
51 radiocarbon reservoir age (Lougheed et al., 2013). Furthermore, it also plays a central role for one of the most
52 widely used dating methods in paleosciences – the radiocarbon dating method. About one third of the data
53 underlying the current radiocarbon calibration curve, IntCal13 (Reimer et al., 2013), obtain their absolute age
54 from climate wiggle-matching.

55 Climate wiggle-matching has the obvious drawback that the leads and lags between different climate records
56 cannot be studied once the records have been forced to align. The approach critically rests on the assumptions,
57 that i) the climate change indeed occurred synchronously everywhere, and that ii) the (sometimes fundamentally
58 different) proxies in question record the changes in a similar way and without intrinsic delays. These
59 assumptions, however, can very rarely be rigorously tested but when they are, ample evidence is revealed that
60 questions their universal validity. Lane et al. (2013) showed that rapid climate change in the North Atlantic
61 region may be time transgressive with regional leads and lags on the order of a century. Nakagawa et al. (2003)
62 argued that the onset of Greenland Interstadial 1e (GI-1e, Rasmussen et al., 2014a) occurred multiple centuries
63 after the associated climate shift in Japan (and subsequent revisions of the underlying timescales (Staff et al.,
64 2013; Bronk Ramsey et al., 2012; Seierstad et al., 2014) did not resolve this conundrum). Buizert et al. (2015)
65 inferred that the Southern Ocean response to DO-events is delayed by about 200 years on average while the
66 atmosphere around Antarctica reacted instantaneously (Markle et al., 2016). Baumgartner et al. (2014) found
67 asynchronicities between ice-core proxies for local Greenland temperature ($\delta^{15}\text{N}$) and the tropical/mid-latitude
68 hydrological cycle (CH_4) during some DO-events. They discussed that the climate changes in polar and low-
69 latitude regions may indeed be synchronous, but that atmospheric CH_4 concentrations rise with a delay during
70 some DO-events because of compensating changes in the source strengths of the northern and southern
71 hemisphere wetlands. Alternatively, their findings can be explained via a real delay between Greenland climate
72 change and the activation of CH_4 source areas during certain DO-events. Fleitmann et al. (2009) reported on
73 timing differences of DO-events in Greenland ice cores and speleothems, albeit largely within dating
74 uncertainties. However, they also found significant differences between speleothem records outside their
75 chronological uncertainties. This is complemented by a recent study showing that the duration of a stadial-
76 interstadial transition can differ by up to 300 years between different East Asian speleothems (Li et al., 2017)
77 emphasizing the questions of whether we should expect the onset, mid-point, or end-point of DO-events to
78 occur simultaneously, as this choice will lead to different results when aligning the records.



79 In this paper, we attempt to provide improved constraints on the paradigm of climate synchronicity. We employ
80 cosmogenic radionuclides as a climate-independent synchronization-tool between the Greenland ice-core
81 timescale (Andersen et al., 2006; Rasmussen et al., 2006; Seierstad et al., 2014; Svensson et al., 2008; Svensson
82 et al., 2006; Vinther et al., 2006) and the U/Th timescale (Broecker, 1963; Edwards et al., 1987; Cheng et al.,
83 2013a) and reduce the absolute dating error of the Greenland ice cores by 50 – 70% back to 45,000 years BP
84 (Before Present, 1950). This allows us to compare the timing of DO-type variability seen in key paleoclimate
85 records at unprecedented precision: The Greenland ice cores and U/Th-dated (sub-)tropical speleothems.

86 **2 Cosmogenic radionuclides as synchronization tools**

87 Cosmogenic radionuclides (such as ^{14}C , ^{10}Be and ^{36}Cl) are produced in a nuclear cascade that is triggered when
88 galactic cosmic rays (GCR) collide with the Earth's atmosphere's constituents (Lal and Peters, 1967). While the
89 GCR flux outside the heliosphere can be assumed to be constant over the past million years (Vogt et al., 1990),
90 the flux arriving at Earth is modulated by the strength of the helio- and geomagnetic fields (Masarik and Beer,
91 1999). Hence, the production rates of cosmogenic radionuclides are inversely related to changes in solar activity
92 and/or the strength of the geomagnetic field. This modulation effect leaves a globally synchronous, externally
93 forced signal in cosmogenic radionuclide records around the world. Hence, they can serve as a powerful
94 synchronization tool for climate archives from different regions. The challenge lies in estimating potential non-
95 production-related impacts on radionuclide concentrations in a given archive that may result from geochemical
96 and meteorological processes.

97 After production, ^{14}C is oxidized to $^{14}\text{CO}_2$ and enters the carbon cycle. Changing ^{14}C production rates thus alter
98 the atmospheric $^{14}\text{C}/^{12}\text{C}$ ratio (expressed as per mille $\Delta^{14}\text{C}$, that is, $^{14}\text{C}/^{12}\text{C}$ corrected for fractionation and decay
99 relative to a standard, denoted Δ in Stuiver & Pollach, 1977). Due to carbon cycle effects, these variations in
100 $\Delta^{14}\text{C}$ are dampened and delayed with respect to the causal production rate changes (Siegenthaler et al., 1980;
101 Roth and Joos, 2013). In addition to variable production rates, changes in the exchange rates between the
102 different carbon pools can alter $\Delta^{14}\text{C}$. The world's oceans in particular have a significantly lower $\Delta^{14}\text{C}$ than the
103 contemporary atmosphere due to their long carbon residence time (Craig, 1957). Thus, variations in the ^{14}C
104 exchange rates between the ocean and the atmosphere will alter atmospheric $\Delta^{14}\text{C}$ independent of production
105 rate changes.

106 ^{10}Be attaches to aerosols and is transported from the stratosphere to the troposphere within 1-2 years (Raisbeck
107 et al., 1981) mainly via mid-latitude tropopause breaks (Heikkilä et al., 2011). It has no active geochemical
108 cycle and so its atmospheric concentration is a more direct recorder of production rate changes compared with
109 $\Delta^{14}\text{C}$. However, ^{10}Be transport and deposition in the troposphere is guided by local meteorology and thus
110 susceptible to changes thereof (Heikkilä and Smith, 2013; Pedro et al., 2011). This can cause variations in ^{10}Be
111 records that are not related to production rate changes. Furthermore, a so-called "polar bias" (i.e., an
112 overrepresentation of polar as opposed to global production rate changes) has been proposed for ice-core records
113 (Bard et al., 1997). This would lead to subdued geomagnetic and enhanced solar modulation of ice-core
114 radionuclide records due to the geometry of the geomagnetic field. However, there is no consensus in different
115 empirical studies and modelling experiments to whether this effect is present and the results may also vary



116 regionally (Bard et al., 1997; Heikkilä et al., 2009a; Pedro et al., 2012; Adolphi and Muscheler, 2016;
117 Muscheler and Heikkilä, 2011; Field et al., 2006).

118 The transport and deposition of ^{36}Cl in its aerosol phase is comparable to ^{10}Be . However, in addition to an
119 aerosol phase, ^{36}Cl also has a gaseous phase (H^{36}Cl) which is likely dominant in the stratosphere (Zerle et al.,
120 1997). In the troposphere, the partitioning between aerosol and gas phase is not well understood. It may vary in
121 space and time (Lukaszczuk, 1994), and can change rapidly depending on pH (Watson et al., 1990). The gaseous
122 H^{36}Cl phase can also be lost from acidic ice in low accumulation sites after deposition which is, however, less
123 relevant for the high accumulation sites studied here (Delmas et al., 2004). In Greenland, similar to ^{10}Be , the
124 dominant deposition process of ^{36}Cl in is wet deposition (Heikkilä et al., 2009b) which is supported by the
125 overall similarity of ^{36}Cl and ^{10}Be variations recorded in ice cores (Wagner et al., 2001b; Muscheler et al.,
126 2005).

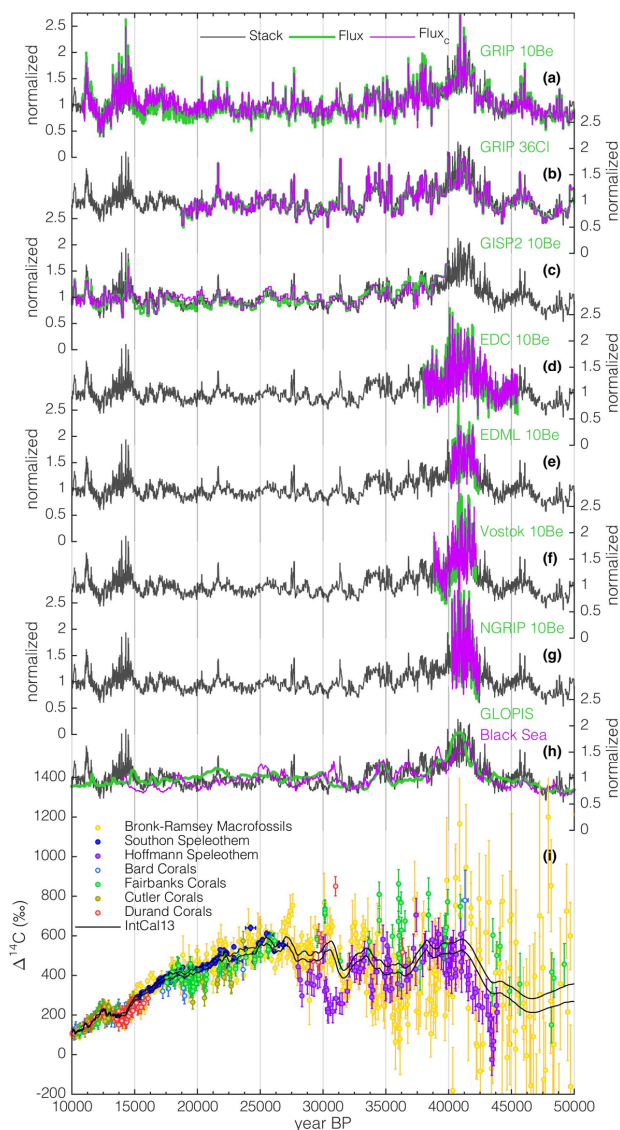
127 As a result, all three radionuclides depend on the same production mechanism which causes their production
128 rates to co-vary globally. This signal can be exploited for global synchronization of paleorecords from natural
129 archives. However, to identify these common changes, their different geochemistry needs to be accounted for. In
130 the case of radiocarbon this is achieved through carbon cycle modelling, to deconvolve the effects of the carbon
131 cycle on the relation between ^{14}C production rates and $\Delta^{14}\text{C}$ (Muscheler et al., 2004). For ^{10}Be and ^{36}Cl , fluxes
132 can be calculated from ice accumulation rates. This provides a first-order correction for changing
133 paleoprecipitation rates on the ice sheet and their influence on the radionuclide concentrations. In reality, aerosol
134 transport to the ice sheet is more complex and depends on changes in transport velocity, pathways and
135 scavenging effects en route (Schüpbach et al., 2018), which are, however, difficult to constrain for ^{10}Be due to
136 its stratospheric origin. Instead, comparisons of fluxes and concentrations to other climate proxies can inform
137 about potential climate influences on ^{10}Be and ^{36}Cl transport and deposition (Adolphi and Muscheler, 2016). It is
138 currently not possible to quantitatively correct either of the radionuclides for these non-production influences
139 since neither past carbon cycle changes nor atmospheric circulation changes are sufficiently well known.
140 However, the potential amplitude of non-production rate changes can be assessed through sensitivity
141 experiments and added as an uncertainty for the production rate signal (Adolphi and Muscheler, 2016; Köhler et
142 al., 2006).

143 The potential of this synchronization tool has been demonstrated multiple times to infer differences between the
144 tree-ring and ice-core timescales (Adolphi and Muscheler, 2016; Muscheler et al., 2014a; Southon, 2002), test
145 the accuracy of the radiocarbon calibration curve (Adolphi et al., 2017; Muscheler et al., 2014b; Muscheler et
146 al., 2008), and synchronize ice cores from both hemispheres (Raisbeck et al., 2017; Raisbeck et al., 2007).

147 **3 Methods & Data**

148 **3.1 Ice-Core Data**

149 The ice-core ^{10}Be and ^{36}Cl data used in this study are shown in figure 1. We focus on records that have been
150 robustly linked to the GICC05 timescale (Andersen et al., 2006; Rasmussen et al., 2006; Seierstad et al., 2014;
151 Svensson et al., 2008; Rasmussen et al., 2008). Hence, the majority of the data stems from the deep Greenland
152 ice cores GRIP, GISP2, and NGRIP. In addition, we use Antarctic ^{10}Be fluxes from EDC, EDML and Vostok



153

154 **Figure 1: Data used in this study. Panel a-g show individual ice-core records of GRIP ^{10}Be (Baumgartner et al.,**
 155 **1997b; Muscheler et al., 2004; Wagner et al., 2001a; Yiou et al., 1997; Adolphi et al., 2014), GRIP ^{36}Cl (Baumgartner**
 156 **et al., 1998; Baumgartner et al., 1997a; Wagner et al., 2001b; Wagner et al., 2000), GISP2 ^{10}Be (Finkel and**
 157 **Nishiizumi, 1997), and ^{10}Be from EDC, EDML, Vostok, and NGRIP (all Raisbeck et al., 2017). Each record**
 158 **represents deposition fluxes (green) and ‘climate corrected’ fluxes (purple, see text). In addition, each panel contains**
 159 **the stack of all ice-core records (black, see text). Panel h: ^{10}Be production rates modelled from two geomagnetic field**
 160 **intensity reconstructions: GLOPIS (green, Laj et al., 2004) and based on Black Sea sediments (purple, Nowaczyk et**
 161 **al., 2013) using the production rate model by Herbst et al. (2016). The ice-core radionuclide stack is shown in black.**
 162 **All records in panel a-h are shown on the GICC05 timescale (Seierstad et al., 2014) and normalized to (i.e., divided**
 163 **by) their mean. Panel i: Absolutely dated ^{14}C data from Lake Suigetsu (yellow, Bronk Ramsey et al., 2012), Hulu**
 164 **Cave (blue, Southon et al., 2012), Bahamas speleothems (purple, Hoffmann et al., 2010), and various tropical coral**
 165 **datasets (Bard et al., 1998; Cutler et al., 2004; Durand et al., 2013; Fairbanks et al., 2005, shown in light blue, olive,**
 166 **red, and green, respectively). The black lines encompass the $\pm 1\sigma$ uncertainties of IntCal13 (Reimer et al., 2013).**



167 that have been anchored to GICC05 by matching solar variability present in all ^{10}Be records, and volcanic tie-
168 points (Raisbeck et al., 2017).

169 By calculating fluxes we make a first order correction for the changing snow accumulation rates between
170 stadials and interstadials and their influence on radionuclide concentrations (Wagner et al., 2001b; Johnsen et
171 al., 1995; Rasmussen et al., 2013; Finkel and Nishiizumi, 1997). The accumulation rates for each ice core are
172 based on their annual layer thickness – derived from their individual timescales – corrected for ice thinning. For
173 the Greenland ice cores this thinning function is based on a 1-D ice flow model (Dansgaard and Johnsen, 1969;
174 Johnsen et al., 1995; Johnsen et al., 2001; Seierstad et al., 2014). For the Antarctic ice cores we use the strain
175 rate derived from the Bayesian ice-core dating effort AICC12 (Veres et al., 2013). These strain rates are
176 inherently uncertain and independently derived accumulation rate estimates differ by up to 10-20% in the glacial
177 (Gkinis et al., 2014; Rasmussen et al., 2013; Guillevic et al., 2013). However, these differences are largely
178 systematic and change only on multi-millennial timescales. The shorter term changes in accumulation rates are a
179 more direct function of the timescale, which is very precise for increments of the core (Rasmussen et al., 2006).
180 This is important to note, as we mainly exploit production rate changes on centennial to millennial timescales
181 for synchronization.

182 To test for additional climate influences on ^{10}Be or ^{36}Cl deposition in the ice cores, we followed the approach by
183 Adolphi and Muscheler (2016): For each ice core we calculated multiple linear regression models using $\delta^{18}\text{O}$
184 and snow accumulation rates as predictors for ^{10}Be (^{36}Cl) fluxes and subtracted the obtained model from the
185 ^{10}Be (^{36}Cl) data. We denote the resulting record as the “climate corrected flux” (Flux_c). This approach may
186 correct climate effects on ^{10}Be (^{36}Cl) deposition insufficiently, or it may over-correct them, so it cannot be
187 assumed per se that the resulting record is more reliable than the original fluxes. Nevertheless, it provides a first
188 order sensitivity test for the ice-core records with respect to climate-related transport and depositional effects on
189 ^{10}Be (^{36}Cl) fluxes.

190 To combine all ice-core records, we calculated their mean (denoted as “Stack”, Fig. 1) using Monte-Carlo
191 bootstrapping (Efron, 1979). Using 7 ice-core records in two versions (flux and flux_c) yields a total number of
192 14 samples. In each iteration, 14 samples are randomly drawn (with replacement, i.e., each record can be drawn
193 multiple times), perturbed within measurement errors, and stacked. Repeating this procedure 1,000 times we
194 obtain an average relative standard deviation of 8% between the derived stacks, which is comparable to the
195 measurement uncertainty of individual measurements but larger than the expected error of the mean which
196 points to systematic differences between the records. For the period where we have data from both hemispheres
197 this standard deviation is only slightly higher (10%). Even though this is only a relatively short period (see Fig.
198 1), it contains multiple DO-events which are expressed differently in Northern and Southern Hemisphere
199 climate. Thus, this agreement can serve as indication that climate effects do not dominate the signal.

200 3.2 Radiocarbon data

201 For the purpose of this study we have to focus on radiocarbon records that are absolutely dated. Furthermore,
202 the length and sampling resolution of the records need to be sufficient to resolve centennial-to-millennial
203 production rate changes. The records that fulfil these criteria are shown in figure 1 and comprise ^{14}C data from
204 various U/Th dated coral records (Bard et al., 1998; Durand et al., 2013; Cutler et al., 2004; Fairbanks et al.,
205 2005), as well as ^{14}C measured in two speleothems (Southon et al., 2012; Hoffmann et al., 2010). In addition,



206 we use the ^{14}C record from Lake Suigetsu (Bronk Ramsey et al., 2012) since the U/Th dated records do not
207 directly reflect atmospheric ^{14}C but the ocean mixed layer (corals) and, in the case of speleothems, a mixture of
208 atmospheric and soil CO_2 , and carbonate bedrock from above the cave. The timescale of the Lake Suigetsu
209 record has been inferred from matching its ^{14}C record to the ^{14}C variations in speleothems, additionally
210 constrained by varve counting (Bronk Ramsey et al., 2012). Hence, it is not truly independently dated. However,
211 similar to ice-core layer counting, this varve count adds constraints especially on centennial timescales, so that
212 $\Delta^{14}\text{C}$ variations on these timescales should be relatively unaffected by this tuning to the speleothem ^{14}C data.
213 Thus, even though the timescale may not be independent, this record can still be used to verify the existence of
214 $\Delta^{14}\text{C}$ variations in the atmosphere seen in the mixed layer records.

215 In addition, we use the available tree-ring records back to 14,000 cal BP in the revised version by Hogg et al.
216 (2016)(not shown in figure 1 for clarity).

217 3.3 Carbon cycle modelling

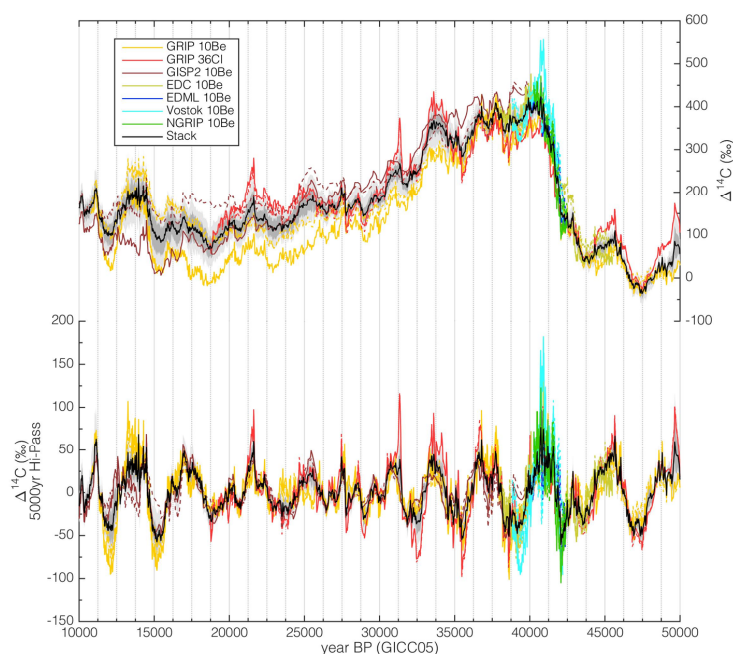
218 To be able to compare ice-core and radiocarbon records directly we have to account for the effects of the carbon
219 cycle. Following earlier studies (Muscheler et al., 2004; Muscheler et al., 2008), we use a box-diffusion carbon
220 cycle model (Siegenthaler et al., 1980) to model $\Delta^{14}\text{C}$ from the ice-core radionuclide records. We assume that
221 ice-core ^{10}Be (^{36}Cl) variations are proportional to ^{14}C production rate changes and model $\Delta^{14}\text{C}$ anomalies from
222 each realization of the ice-core stack, as well as the single ice-core records (Fig. 2). It can be seen that the
223 modelled $\Delta^{14}\text{C}$ records from the individual ice-core records differ in their long-term trends since the carbon
224 cycle integrates over time so that relatively small but systematic differences in the radionuclide fluxes (possibly
225 arising from uncertainties in the strain rates) have a significant effect on longer time scales. However, all records
226 show the same overall evolution of $\Delta^{14}\text{C}$. Furthermore, especially when subtracting the long-term trend and
227 isolating variations on timescales shorter than 5000 years, the agreement is very high (on average within 15% at
228 1σ , Fig. 2b), which is the part of the signal that we will be exploiting in our synchronization effort.

229 3.3.1 Production rate ratio

230 Modeling $\Delta^{14}\text{C}$ values from ^{10}Be measurements is based on the assumption that ^{10}Be and ^{14}C production rate
231 changes are proportional to each other. However, different production rate models differ in their sensitivity of
232 ^{14}C and ^{10}Be production rate changes to variations in the geomagnetic field (Cauquoin et al., 2014). For a given
233 geomagnetic field change, the production rate model by Masarik and Beer (2009, 1999) yields 30-50% lower
234 ^{10}Be production rate changes than the calculations by Poluianov et al. (2016) and Herbst et al. (2016). For ^{14}C on
235 the other hand, all models yield roughly similar amplitudes. This leads to differences in the $^{14}\text{C}/^{10}\text{Be}$ production
236 rate ratio for a given change in the geomagnetic field. If Masarik and Beer (1999) are correct, the variations in
237 ice-core ^{10}Be records have to be upscaled by 30-50% to be proportional to ^{14}C production rate changes while no
238 such scaling is necessary when the other production rate models are used. In addition, the amplitudes in ^{14}C and
239 ^{10}Be may differ due to the presence of polar bias (see section 2). If this effect was present, then geomagnetic
240 field changes should cause bigger variations in ^{14}C than ^{10}Be .

241 Since the presence of a polar bias is debated and the physical reason for the differences between the production
242 rate models is unresolved, we chose an empirical approach to scale the ice-core record appropriately:

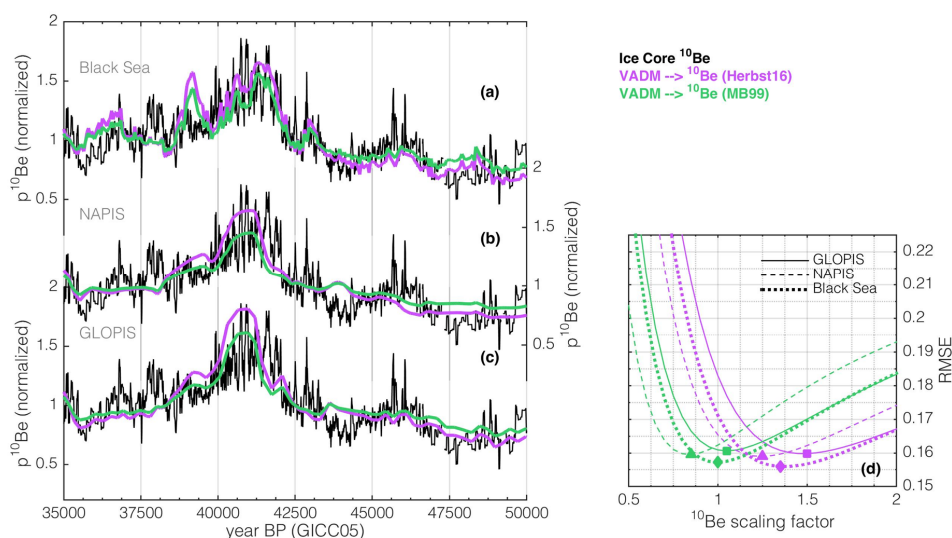
243



244

245 **Figure 2: Modelled $\Delta^{14}\text{C}$ anomalies from individual ice-core records (see legend, solid lines are based on radionuclide**
 246 **fluxes while dashed lines are inferred from flux_x) and the realizations of the ice-core stack (black line shows the mean**
 247 **of all realizations, dark and light grey shading encompass 68.2 and 95.4% probability ranges). The top panel shows**
 248 **the unfiltered model output. The bottom panel displays the records after variations with frequencies $< 1/5000\text{a}^{-1}$ have**
 249 **been subtracted (FFT-based filter).**

250 We use three geomagnetic field intensity reconstructions around the Laschamp geomagnetic field minimum (Laj
 251 et al., 2004; Laj et al., 2000; Nowaczyk et al., 2013) and calculate the resulting ^{10}Be production rate changes
 252 using the production rate models by Masarik and Beer (1999) and Herbst et al. (2016) (Fig. 3 a-c).
 253 Subsequently, we scale the ice-core ^{10}Be record to minimize the root mean square error (RMSE) between ice-
 254 core and geomagnetic field-based records (Fig. 3d). It can be seen that the RMSE reaches a minimum for a ^{10}Be
 255 scaling factor of ~ 1 (for Masarik and Beer, 1999) and ~ 1.3 (for Herbst et al., 2016). This represents a fortunate
 256 coincidence; irrespective of which production rate model is used, the amplitude of the ice-core ^{10}Be variations
 257 has to be increased by approximately 30% to match ^{14}C . If the production rate model by Masarik and Beer is
 258 used, then the amplitude of the ice-core ^{10}Be record is in agreement with geomagnetic field data, but due to the
 259 higher production sensitivity of ^{14}C (see above), ^{10}Be variations have to be increased by $\sim 30\%$. Similarly, if the
 260 production rate model by Herbst et al. is used, then the amplitude of the ice-core ^{10}Be record is 30% smaller
 261 than implied by geomagnetic field data (possibly due to a polar bias), while the sensitivity of ^{14}C and ^{10}Be is the
 262 same. Again, the net effect is the ^{10}Be variations have to be scaled up by 30% for the comparison to ^{14}C .



263

264 **Figure 3: Comparison of ice-core-based and geomagnetic-field-based reconstructions of ^{10}Be production rates.** Panel
 265 a-c show the ice-core stack (black) in comparison to ^{10}Be production rates based on geomagnetic field reconstructions
 266 and 2 different production rate models (Herbst et al. (2016) in pink and Masarik and Beer (1999) in green). Panel a,
 267 the Black Sea geomagnetic field record (Nowaczyk et al., 2013), Panel b, the NAPIS geomagnetic field stack (Laj et
 268 al., 2000), and Panel c, the GLOPIS geomagnetic field stack (Laj et al., 2004). Panel d shows the RMSE between the
 269 ice-core data and the geomagnetic-field-based records when variations in the ice-core record are scaled by different
 270 factors (x-axis). The colours correspond to the production rate models. The line styles indicate the geomagnetic field
 271 records (see legend) and the symbols denote the RMSE minima.

272 3.3.2 The state of the carbon cycle

273 As mentioned in section 2, a quantification of transient carbon cycle changes and their influence on $\Delta^{14}\text{C}$ is
 274 challenged by insufficient knowledge of inventories and processes. The contribution of single processes to $\Delta^{14}\text{C}$
 275 changes over the last glacial cycle is likely within 30% and, due to compensating effects, also their combination
 276 is likely not bigger than 40% (Köhler et al., 2006). Here we use the Laschamp event to estimate the state of the
 277 ocean ventilation around 40 ka BP.

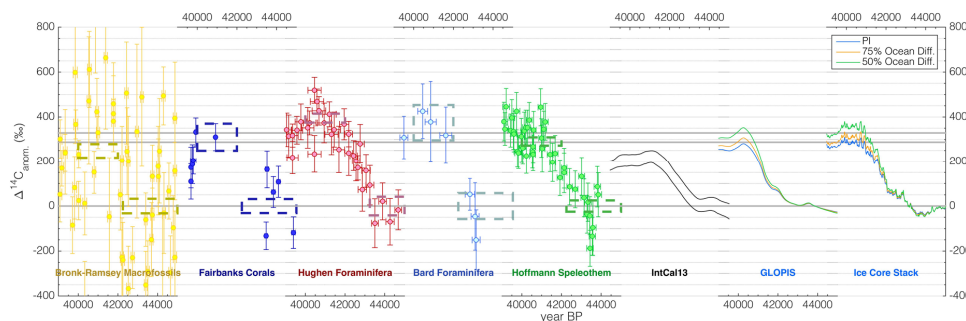
278 The datasets underlying IntCal13 all show an increase of about 320‰ in $\Delta^{14}\text{C}$ into the Laschamp event (Fig. 4),
 279 albeit at different absolute levels (see Fig. 1). This is ~100% more than the compiled IntCal13 curve itself
 280 implies. This disagreement can be explained by differences in timing and absolute $\Delta^{14}\text{C}$ between the different
 281 datasets leading to smoothing and dampening of $\Delta^{14}\text{C}$ variations during the construction of IntCal13. Also,
 282 geomagnetic field changes yield a $\Delta^{14}\text{C}$ change more in line with the individual ^{14}C datasets than with IntCal13,
 283 even when assuming a preindustrial carbon cycle.

284 To estimate the mean state of the carbon cycle during this period, we run our carbon cycle model with different
 285 (constant) values of ocean diffusivity. We find that modelled and measured $\Delta^{14}\text{C}$ around the Laschamp event
 286 match best in amplitude when we run the model under conditions where ocean ventilation is reduced to ~75% of
 287 its preindustrial value (Fig. 4). This is in broad agreement with previous modelling experiments (Köhler et al.,
 288 2006; Roth and Joos, 2013) and proxy data (Henry et al., 2016).

289 In the following, we will use this estimate for the parameterization of our model. As mentioned above, a
 290 transient adjustment of carbon cycle parameters is uncertain and will hence not be attempted. Instead, we
 291 ascribe an associated uncertainty to the modelled $\Delta^{14}\text{C}$ based on the carbon cycle sensitivity experiments by



292 Köhler et al. (2006). Furthermore, it should be noted, that by only using (filtered) $\Delta^{14}\text{C}$ anomalies as
 293 synchronization targets, we i) avoid systematic carbon cycle influences on $\Delta^{14}\text{C}$ levels, and ii) minimize
 294 transient carbon cycle related changes in $\Delta^{14}\text{C}$ (Adolphi and Muscheler, 2016).



295

296 **Figure 4: The Laschamp event in measured and modelled $\Delta^{14}\text{C}$.** The 6 panels to the left show $\Delta^{14}\text{C}$ anomalies from
 297 macrofossils from Lake Suigetsu (yellow, Bronk Ramsey et al., 2012), tropical corals (blue, Fairbanks et al., 2005),
 298 foraminifera from Cariaco Basin sediments (red, Hughen et al., 2006), foraminifera from Iberian Margin sediments
 299 (light blue, Bard et al., 2013), Bahamas speleothems (green, Hoffmann et al., 2010), and IntCal13 (black, Reimer et
 300 al., 2013). The two panels on the right show modelled $\Delta^{14}\text{C}$ using the GLOPIS (Laj et al., 2004) geomagnetic field
 301 record as well as the ice-core stack as production rate inputs. The different coloured lines reflect different carbon
 302 cycle scenarios (see legend, PI denotes pre-industrial). The conversion of geomagnetic field intensity to ^{14}C production
 303 rate is based on the production rate model by Herbst et al. (2016). Note, that the amplitude of the ^{10}Be variations have
 304 been increased by 30% as discussed in section 3.3.1.

305

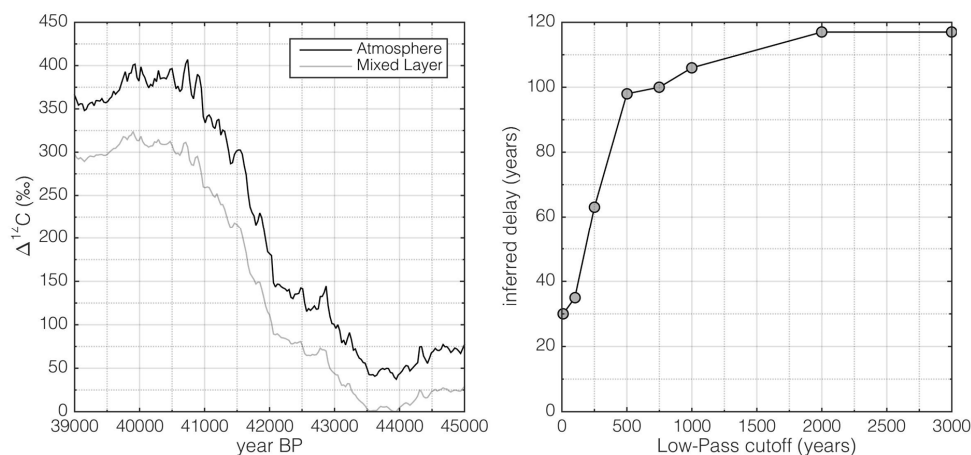
306 3.4 Synchronization – effects of the carbon cycle and the archive

307 The synchronization method follows Adolphi and Muscheler (2016) and is outlined and tested in detail therein.
 308 In brief, sections of modelled (ice-core based) $\Delta^{14}\text{C}$ anomalies are compared to the measured $\Delta^{14}\text{C}$. For our
 309 analysis we employ high-frequency changes in $\Delta^{14}\text{C}$ since carbon cycle changes have only limited effects on
 310 atmospheric $\Delta^{14}\text{C}$ on shorter time scales (Adolphi and Muscheler (2016). Similarly, as shown in figure 2, the
 311 agreement of the different ice-core records is better on shorter timescales. In this study, we employ two types of
 312 high pass filtering: a FFT-based high-pass filter and simple linear detrending. The choice of filter is based on the
 313 data sampling resolution. For the highly resolved tree-ring data we use the FFT filter, while the lower resolved
 314 and more unevenly sampled coral/speleothem/macrofossil data is filtered by linear detrending to avoid the
 315 interpolation to equidistant resolution required for FFT analysis. The exact frequencies and window lengths are
 316 given in the results section. Using the same statistics as for radiocarbon wiggle-match dating (Bronk Ramsey et
 317 al., 2001), we then infer a probability density function (PDF) for the timescale difference between the modelled
 318 and measured $\Delta^{14}\text{C}$ records. For details of the statistics of this methodology we refer the reader to Adolphi and
 319 Muscheler (2016). Here we focus instead on additional uncertainties that arise when comparing modelled
 320 atmospheric $\Delta^{14}\text{C}$ to ^{14}C records from the ocean mixed layer (corals) or speleothems.

321 $\Delta^{14}\text{C}$ variations in the atmosphere are dampened and delayed compared to the causal production rate changes.
 322 Both factors, attenuation and delay, depend on the frequency of the production rate change (Roth and Joos,
 323 2013; Siegenthaler et al., 1980). The dampening is largest at high frequencies and decreases with longer periods.
 324 On the other hand, the apparent peak-to-peak delay between sinusoidal production rate changes and the resulting



325 $\Delta^{14}\text{C}$ change is increasing with increasing wavelengths. Similar effects occur when comparing atmospheric and
326 oceanic $\Delta^{14}\text{C}$ changes to each other: the ocean reacts to atmospheric $\Delta^{14}\text{C}$ changes with a delayed and dampened
327 response that is wavelength dependent. Hence, we need to take these factors into account when comparing a
328 modelled atmospheric $\Delta^{14}\text{C}$ record to mixed layer marine records. However, the frequency dependence of the
329 attenuation and delay makes it difficult to explicitly correct for this since atmospheric $\Delta^{14}\text{C}$ changes vary on
330 different time scales simultaneously. Furthermore, the coral records vary in their sampling frequency and often
331 it is not precisely known over how much time an individual ^{14}C sample integrates.
332 Figure 5 shows a sensitivity test regarding these effects. We modelled $\Delta^{14}\text{C}$ from the ice-core stack around the
333 Laschamp event and compared the atmospheric $\Delta^{14}\text{C}$ to the mixed layer $\Delta^{14}\text{C}$ in the model. To simulate the
334 effect of varying averaging effects of the coral samples, we low-pass filtered the mixed layer signal with
335 increasing cut-off wavelengths. For each filter, we then inferred the apparent delay between the mixed layer
336 (i.e., the “coral”) and the atmosphere. In doing so we infer that even though the signal is dominated by a long
337 lasting $\Delta^{14}\text{C}$ increase, the inferred delay is small (~ 30 years) as long as the coral samples do not integrate over
338 long times. Only when assuming that each coral sample averages over more than 1,000 years we infer delays of
339 about 120 years. Nevertheless, this experiment also shows that within reasonable bounds of averaging, the delay
340 of mixed layer to atmospheric signal is limited

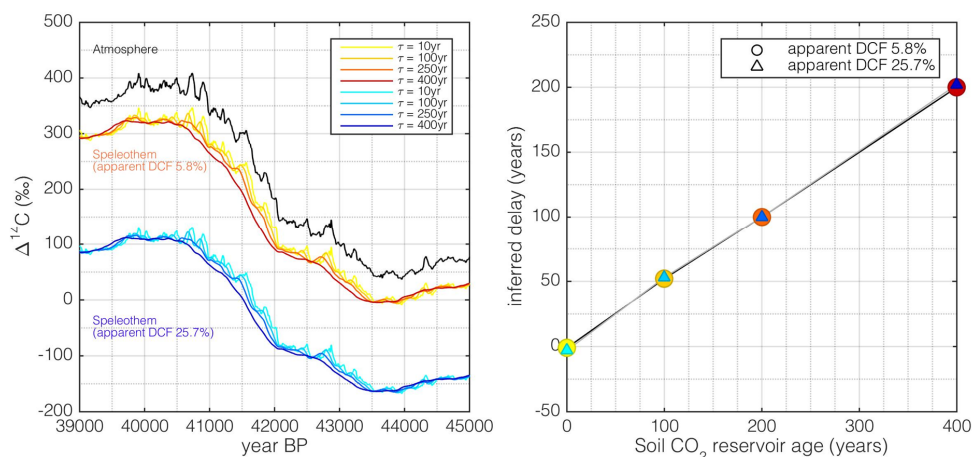


341
342 **Figure 5: The delay between $\Delta^{14}\text{C}$ in the atmosphere and ocean mixed layer. The left panel shows modelled $\Delta^{14}\text{C}$**
343 **from the ice-core stack around the Laschamp event. The modelled atmospheric $\Delta^{14}\text{C}$ is shown in black while ocean**
344 **mixed layer is shown in grey. The right hand panel shows the inferred delay from our synchronization method when**
345 **comparing the atmospheric to the mixed layer signal for different low-pass filters of the mixed layer signal (x-axis).**

346
347 The speleothem $\Delta^{14}\text{C}$ reacts differently than the ocean mixed layer. The so-called dead carbon fraction (DCF) of
348 a speleothem consists of two main contributors: i) respired soil organic matter that is older (in ^{14}C years) than
349 the atmospheric ^{14}C signal, and ii) carbonate bedrock that contains no ^{14}C . Applying the model of Genty and
350 Massault (1999), we model speleothem $\Delta^{14}\text{C}$ using different assumptions on the age of the respired soil organic
351 matter and fraction of carbonate bedrock in drip water CO_2 . We do this for 2 examples: i) a speleothem with an
352 apparent DCF (i.e., offset from the atmosphere) of 5.8% (resembling the Hulu Cave speleothem record by
353 Southon et al., 2012) and ii) a speleothem with an apparent DCF of 25.7% (resembling the Bahamas speleothem



354 by Hoffmann et al., 2010). By assuming different ages of the soil respired carbon ($\tau = 10 - 400$ years, see Fig.
355 6), we adjust the fraction of ^{14}C -free CO_2 so that the apparent DCF for each speleothem is matched. The age of
356 the soil respired carbon is defined following Genty and Massault (1999): if, for example, $\tau = 100$ years, then the
357 activity of the soil respired CO_2 is the mean of the atmospheric activity over the past 100 years prior to sampling
358 (also accounting for decay within these 100 years). For simplicity we assume a uniform age distribution for the
359 soil respired carbon. Subsequently, we compare the modelled speleothem $\Delta^{14}\text{C}$ to the original atmospheric input
360 using our synchronization method and plot the inferred delay (Fig. 6, right panel). From this experiment it can
361 be seen that the controlling factor on the inferred delay is the age of the soil respired matter that acts as an
362 integrator (low-pass filter) of the atmospheric ^{14}C signal. The fraction of ^{14}C -free carbonate has no influence on
363 the lag between $\Delta^{14}\text{C}$ changes in the atmosphere and the speleothem, but only dampens the amplitude of the
364 corresponding change. Realistic ages of soil respired carbon differ from region to region but even though some
365 slow cycling fractions of soil organic matter may be up to several thousand years old (Trumbore, 2000), the
366 major contributors to soil CO_2 are considerably younger and in the order of decades (Genty et al., 2001;
367 Fohlmeister et al., 2011).
368 From these experiments we conclude that our systematic matching uncertainties to coral and speleothem records
369 are probably below 100 years. We note that this uncertainty is asymmetric since the ocean/speleothem signal
370 cannot lead the atmosphere and so the offset is unidirectional.
371



372
373 **Figure 6: Effect of varying ages of soil respired CO_2 and fractions of CO_2 from ^{14}C -dead carbonate on the $\Delta^{14}\text{C}$ in**
374 **speleothems. The left panel shows atmospheric modelled $\Delta^{14}\text{C}$ from the ^{10}Be stack (black) and two modelled**
375 **speleothem scenarios with a net DCF of 5.8% (warm colours) and 25.7% (cold colours). For each speleothem, a**
376 **number of different ages for the respired soil organic matter have been assumed (see legend) and the input of ^{14}C -free**
377 **CO_2 from carbonate has been adjusted to obtain the correct apparent DCF value between 39-40.5 ka BP. The right**
378 **hand panel shows the inferred delay when we apply our synchronization method to match the atmospheric $\Delta^{14}\text{C}$ to**
379 **the speleothem record.**

380 3.5 Change-point detection in climate records

381 To assess the synchronicity of abrupt climate changes between the climate records after the synchronisation we
382 use a probabilistic approach to detect their onsets in the individual records. The employed model describes the



383 abrupt changes as a linear transition between two constant states. To account for long-term fluctuations in the
 384 climate records, deviations from the transition are described as autocorrelated noise. The approach and inference
 385 procedure are described in more detail in Erhardt et al. (in prep). The model is fitted independently to windows
 386 of the individual datasets (table 1 & Fig. 13) around the rapid transitions on their individual timescales. The
 387 apparent delays between the inferred onsets of the transitions in the different records are then compared,
 388 propagating the respective uncertainties. For each record, only events that are well expressed and measured in
 389 high resolution have been fitted.

390 **Table 1. Change-point detection window for each record. For each investigated climate event and record, the change-**
 391 **point detection algorithm has been applied between t1 and t2. The windows have been defined visually, ensuring a**
 392 **sufficient amount of data prior to and after the transition. For each record, only events that are well expressed in the**
 393 **climate proxy records at high resolution have been investigated. For the ice-core record t1 and t2 typically encompass**
 394 **500 years prior to and after the nominal transition ages by Rasmussen et al. (2014a). The exact values have been**
 395 **adjusted to exclude overlap with other transitions where necessary (Erhardt et al. in prep).**

Event	GICC05 (yr BP)	MCE	Hulu d18O		Sofular d18O		Sofular d13C		ElCondor d18O		Diamante d18O	
			t1	t2	t1	t2	t1	t2	t1	t2	t1	t2
Holocene	11653	99	12453	10503	12703	10703	12703	11003	12453	11203	13403	11203
GI-1e	14642	186	15442	13942	15442	13942	15442	13942	15442	14192	16392	14192
GS-3 Dust Peak	24130	645	25380	24080	-	-	-	-	-	-	25780	24630
GI-3	27730	832	28580	27680	28780	27880	28780	27780	-	-	29030	28080
GI-4	28850	898	30100	28900	30150	29400	30150	29200	29900	29000	30100	29100
GI-5.1	30790	1008	31540	30790	-	-	-	-	31590	30740	32040	30840
GI-5.2	32450	1132	33300	32200	33100	32400	33300	32200	33250	32000	33050	32450
GI-6	33690	1195	34590	33640	34740	33690	34990	33540	34240	33490	-	-
GI-7c	35430	1321	36680	34980	36380	35480	36380	35230	36230	34880	36480	34980
GI-8c	38170	1449	39420	37420	39420	37220	39120	37220	39220	37220	-	-
GI-9	40110	1580	40860	40060	40960	39960	41160	39960	-	-	-	-
GI-10	41410	1633	42110	41060	42460	41590	42460	41460	42210	40960	-	-
GI-11	43290	1736	44240	42940	44840	43540	-	-	44040	42440	-	-

396

397 4 Time scale differences between GICC05 and the U/Th timescale

398 In the following sections we will show the synchronization results for different time windows. We focus our
 399 analysis on three distinct windows: 10-14 ka BP, 18-25 ka BP and 39-45 ka BP. The youngest window is
 400 defined by the presence of high-resolution tree-ring data for ^{14}C back to 14 ka BP. Going further back in time it
 401 becomes increasingly challenging to unequivocally identify common structures in the various $\Delta^{14}\text{C}$ records that
 402 are suitable for synchronization because the resolution of the individual records decreases back in time while
 403 their differences to each other are growing steadily (see Fig. 1i). Hence, we focus on the well-known Laschamp
 404 event around 41 ka BP, and the period between 18-25kaBP, i.e., preceding the major carbon cycle changes
 405 associated with the deglaciation. We omit the period between 25-39 ka BP. As discussed in Reimer et al. (2013)
 406 and seen in figure 1i there is substantial disagreement between the datasets underlying IntCal13 at that time that
 407 are impossible to reconcile within their respective age and/or ^{14}C uncertainties. Hence, also any structure in the
 408 $\Delta^{14}\text{C}$ records may be unreliable and thus, lead to erroneous synchronization results.

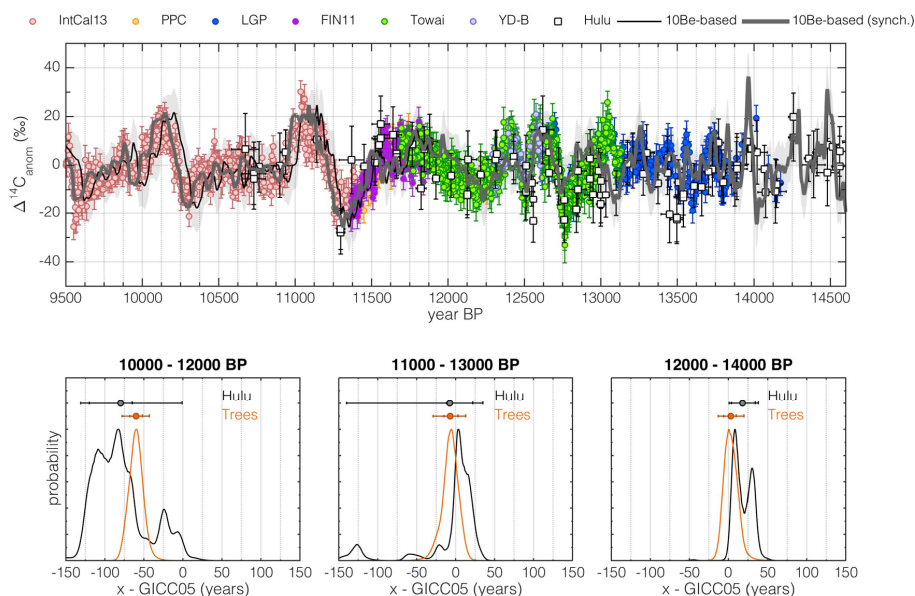
409 4.1 10,000 – 14,000 years BP

410 In the 10-14 ka BP interval, we synchronize the ice-core stack to high-resolution tree-ring and speleothem $\Delta^{14}\text{C}$
 411 data (Fig. 7). The high sampling resolution of the ^{14}C records allows us to focus on centennial-to-millennial



412 $\Delta^{14}\text{C}$ changes (<1000 years) where carbon cycle influences on $\Delta^{14}\text{C}$ can be expected to be small (Adolphi and
 413 Muscheler, 2016). In concordance with earlier studies (Muscheler et al., 2014a) we find that GICC05 is ~65
 414 years older than the tree-ring timescale at the onset of the Holocene, but that this offset vanishes over the course
 415 of the Younger Dryas interval.

416 While Muscheler et al. (2014a) argued that this changing offset may be in part due to errors in the timescale of
 417 the floating Late Glacial Pines, we can now support this change in the timescale-difference through the U/Th
 418 dated speleothems: The synchronization of the ice-core stack to the H82 speleothem from Hulu Cave (Southon
 419 et al., 2012) leads to fully consistent results as inferred from the tree-rings. This indicates that the most likely
 420 explanation is an ice-core layer counting bias, i.e. that the GICC05 time scale suggests too old ages at the onset
 421 of the Holocene, but is accurate within a few decades during GI-1.



422
 423 **Figure 7: Synchronization of GICC05 to tree-ring and Hulu Cave records during the last deglaciation. Top panel:**
 424 **Ice-core based modelled $\Delta^{14}\text{C}$ anomalies on the original GICC05 timescale (thin black line, light grey shading**
 425 **encompasses the $\pm 10\%$ uncertainty ($\pm 1\sigma$) of the modelled $\Delta^{14}\text{C}$, based on the carbon-cycle sensitivity experiments by**
 426 **Adolphi & Muscheler (2016)) and synchronized timescale (bold grey line). Tree-ring data underlying IntCal13 are**
 427 **shown in pink. Revised Northern Hemisphere tree-ring data according to Hogg et al. (2016) are shown in orange**
 428 **(Preboreal Pines), dark blue (Late Glacial Pine) and light blue (Younger Dryas-B chronology). New kauri $\Delta^{14}\text{C}$ data**
 429 **by Hogg et al. (2016) is shown in purple (FIN11) and green (Towai). Hulu Cave H82 $\Delta^{14}\text{C}$ data are shown as white**
 430 **squares. All symbols are shown with $\pm 1\sigma$ error bars. All data are FFT-filtered to isolate $\Delta^{14}\text{C}$ variations on timescales**
 431 **<1000 years. The lower three panels show inferred probability distributions of timescale differences between GICC05**
 432 **and tree-rings (orange) and Hulu Cave (black). The symbols and error bars denote means, and 68.2% and 95.4%**
 433 **confidence intervals of the inferred timescale difference. Each of the lower panels refers to a 2000-year subsection**
 434 **of the data indicated at the top of each panel.**

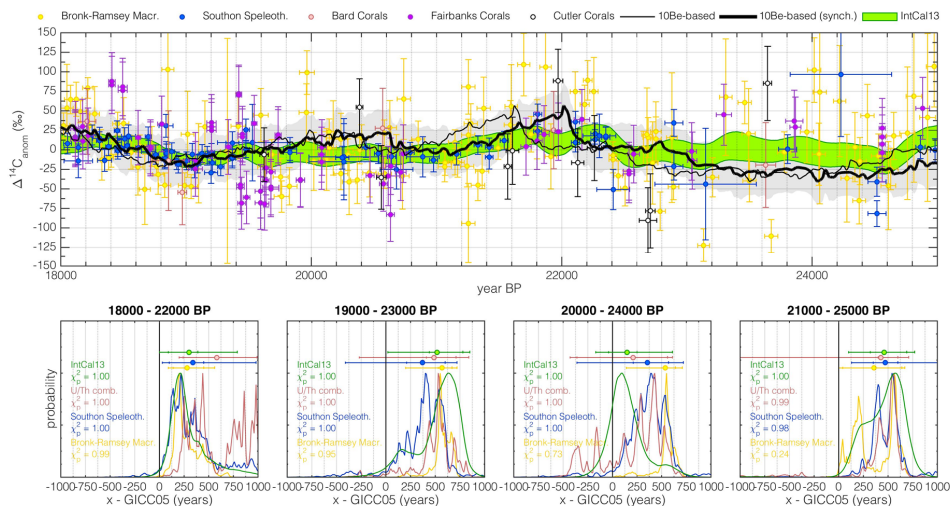
435 Interestingly, we do not observe any significant differences between the results stemming from tree-rings and
 436 the speleothem records. As shown in section 3.4, we could expect a delay in the speleothem $\Delta^{14}\text{C}$ compared to
 437 the atmosphere if the respired soil organic carbon contribution to the soil CO_2 was very old. This would result in
 438 GICC05 appearing older in comparison to the speleothem than relative to the tree rings. The lack of this delay
 439 implies that the majority of the respired soil organic carbon at Hulu Cave must be younger than ~100 years (see
 440 Fig. 6). This is supported by the fact that the centennial $\Delta^{14}\text{C}$ variations in the tree-ring and speleothem data



441 have the same amplitude (Fig. 7). If old organic carbon significantly contributed to the soil CO₂, we would
 442 instead expect to see a stronger smoothing of short-term $\Delta^{14}\text{C}$ variations.

443 4.2 18,000 – 25,000 years BP

444 Due to the irregular and lower sampling resolution of the ^{14}C records beyond 15,000 cal BP, we chose to
 445 linearly detrend each data set (instead of band-pass filtering) to remove offsets between the different ^{14}C
 446 datasets and highlight common variability. Furthermore, we have to increase the length of the comparison data
 447 windows to 4,000 years to ensure sufficient structure in the ^{14}C sequences entering the comparison. Each
 448 window is detrended separately in the analysis to isolate short-term $\Delta^{14}\text{C}$ variability. We note however, that
 449 detrending each ^{14}C dataset over the entire timeframe (18-25 ka BP) instead does not alter the results
 450 significantly. Compared to the high-frequency $\Delta^{14}\text{C}$ changes studied between 10-14 ka BP, the longer-term
 451 variations used for synchronization here may have been increasingly affected by carbon-cycle changes. To
 452 account for this, we increase the uncertainty estimate of the modelled $\Delta^{14}\text{C}$ changes to $\pm 30\%$ ($\pm 1\sigma$), which is
 453 sufficiently large to account for estimated carbon-cycle-driven $\Delta^{14}\text{C}$ changes from modelling experiments
 454 during the entire glacial (Köhler et al., 2006). We note that this is a conservative estimate, given that during this
 455 period neither modelling (Köhler et al., 2006; Muscheler et al., 2004), nor data (Eggleston et al., 2016) suggest
 456 large carbon-cycle changes.



457

458 **Figure 8: Synchronization results between 18,000 and 25,000 years BP.** Top panel: The thin black line shows the
 459 modelled $\Delta^{14}\text{C}$ curve based on the ice-core stack on its original timescale. The bold black line and grey shading show
 460 the synchronized ice-core record including assumed $\pm 1\sigma$ uncertainties of $\pm 30\%$. The different coloured symbols
 461 indicate various ^{14}C datasets underlying IntCal13, which is shown as the green envelope. Lower panels: Each panel
 462 shows PDFs of the inferred timescale difference between the ice-core stack and IntCal13 (green), a combination of all
 463 U/Th-dated records (speleothems/corals, pink), the H82 speleothem (blue), and Lake Suigetsu (yellow). Symbols of
 464 similar colour show the inferred mean and 68.2% and 95.4% confidence intervals. Colour-coded text indicates χ^2
 465 probabilities for the goodness of fit between modelled and measured $\Delta^{14}\text{C}$ curves after synchronization. Small (e.g.,
 466 < 0.1) values would indicate significant disagreement. Note that all χ^2 probabilities are relatively high, indicating that
 467 our uncertainty estimate for the modelled $\Delta^{14}\text{C}$ is very conservative. Each of the lower panels refers to a specific
 468 subsection of the data indicated at the top of each panel.

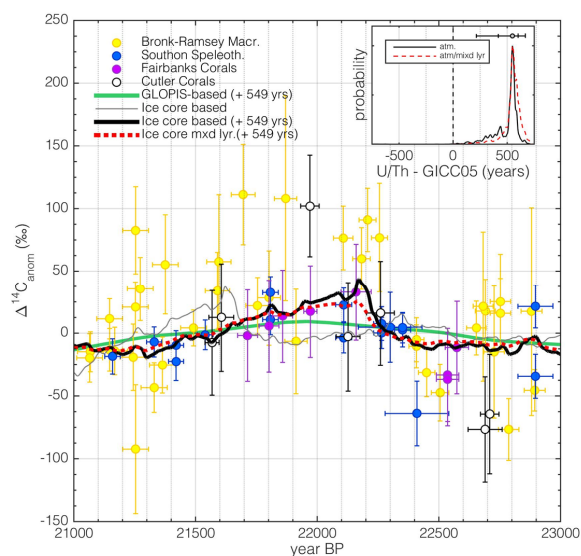
469 It can be seen in figure 8 that it is challenging to infer robust co-variability in multiple ^{14}C records. However, the
 470 millennial evolution of $\Delta^{14}\text{C}$ does show common changes in the 18-25 ka BP interval. Synchronizing the ice-



471 core stack to data from i) Hulu Cave H82 speleothem, ii) Lake Suigetsu macrofossils, iii) the IntCal13 stack or
 472 iv) a combination of all U/Th dated records (speleothems/corals) leads to consistent results within uncertainties
 473 for each choice of time windows: all records imply that GICC05 shows younger ages compared to the ^{14}C
 474 records around this time.

475 The most significant structure that is present in all measured and modelled ^{14}C records during this time is the
 476 centennial $\Delta^{14}\text{C}$ increase around 22.1kaBP (see Fig. 9). Comparing the ice-core stack to $\Delta^{14}\text{C}$ between 21-
 477 23kaBP indicates an offset of ~ 550 years between GICC05 and the U/Th timescale around this time (GICC05
 478 being younger). To account for the potential delay of coral and speleothem $\Delta^{14}\text{C}$ compared to the atmosphere,
 479 we also modelled the mixed layer $\Delta^{14}\text{C}$ signal from the ice-core stack and synchronized this signal to the
 480 measured ^{14}C data (Fig. 9). As discussed in section 3.4, we find very little difference in the inferred timing since
 481 the $\Delta^{14}\text{C}$ variation is relatively rapid (centuries). Comparing the $\Delta^{14}\text{C}$ anomalies to geomagnetic field data
 482 shows that a small part of the longer-term development of this structure is probably driven by geomagnetic field
 483 changes. The amplitude ($\sim 50\%$) and short duration (centuries) of the $\Delta^{14}\text{C}$ increase, however, suggest that this
 484 change is mainly driven by a series of strong solar minima, comparable to the Grand Solar Minimum period
 485 around the onset of the Younger Dryas (Muscheler et al., 2008).

486



487

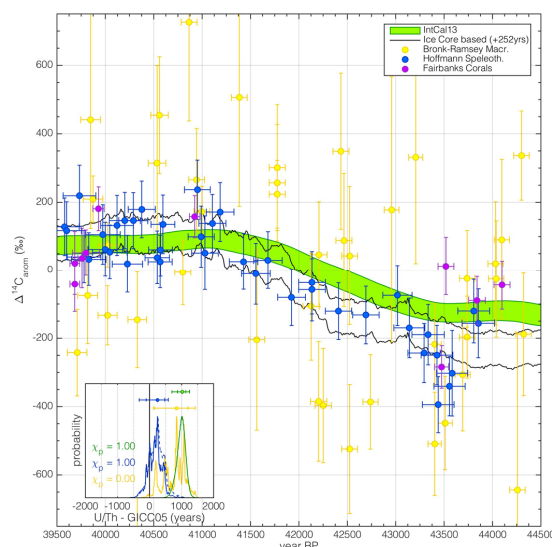
488 **Figure 9: Close-up of measured and modelled $\Delta^{14}\text{C}$ anomalies between 21 and 23 ka BP.** The thin grey line shows
 489 modelled atmospheric $\Delta^{14}\text{C}$ from the ice-core stack on the GICC05 time scale. The bold black and dashed red lines
 490 show the modelled atmospheric and ocean mixed layer $\Delta^{14}\text{C}$ curves after synchronization to the ^{14}C records (yellow:
 491 Lake Suigetsu; blue: Hulu Cave; purple and white: corals). The inset panel shows the PDF of the inferred timescale
 492 difference between GICC05 and the combination of all ^{14}C records. The black line is based on using only the
 493 modelled atmospheric $\Delta^{14}\text{C}$. The red dashed line is based on comparing coral and speleothem data to the modelled
 494 mixed-layer $\Delta^{14}\text{C}$, and Lake Suigetsu data to modelled atmospheric $\Delta^{14}\text{C}$. The green line shows modelled $\Delta^{14}\text{C}$ based
 495 on geomagnetic field changes.

496



497 4.3 39,000 – 45,000 years BP

498 Our oldest tie-point is the previously discussed Laschamp event around 41 ka BP. The only independently and
 499 absolutely dated ^{14}C record around this time that has a sufficient sampling resolution is the Bahamas speleothem
 500 by Hoffmann et al. (2010). While offset in absolute $\Delta^{14}\text{C}$ (see Fig. 1), the U/Th-dated coral data supports the
 501 amplitude and timing of the $\Delta^{14}\text{C}$ increase seen in the speleothem even though precise synchronization is
 502 hampered by the low sampling resolution of the corals. The Lake Suigetsu record is characterized by large
 503 uncertainties and scatter around this time. As discussed in section 3.3.2, IntCal13 is smoothed around
 504 Laschamp, having a smaller amplitude and a less sharp rise in $\Delta^{14}\text{C}$. For this tie-point, we merely remove the
 505 error-weighted mean between 39-45 ka BP from each dataset, since detrending would remove the largest part of
 506 the signal. Hence, there are large $\Delta^{14}\text{C}$ modelling uncertainties associated with unknown carbon-cycle changes,
 507 and we assume a Gaussian $\pm 1\sigma$ error of 50‰, which we consider conservative since sensitivity experiments
 508 imply that the impact of carbon cycle changes on $\Delta^{14}\text{C}$ was likely below 40‰ (Köhler et al., 2006).



509

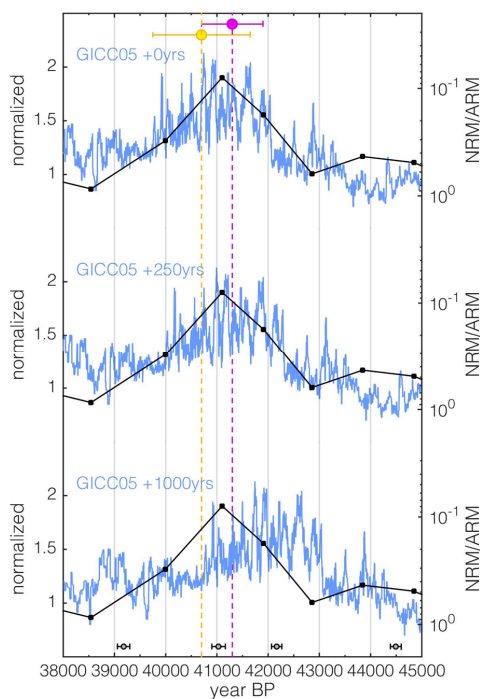
510 **Figure 10. Synchronization of ^{10}Be and ^{14}C around the Laschamp event. The black lines encompass the modelled**
 511 **$\Delta^{14}\text{C}$ anomalies ($\pm 1\sigma$) from the ice-core data shifted by +252 yrs (68.2% confidence interval = -103 to 477 yrs)**
 512 **according to their best fit to the speleothem ^{14}C data. The green patch shows the $\pm 1\sigma$ envelope of IntCal13. The blue**
 513 **and purple symbols show $\Delta^{14}\text{C}$ from Bahamas speleothem, and corals, respectively. The yellow symbols show $\Delta^{14}\text{C}$**
 514 **anomalies based on Lake Suigetsu macrofossils. All datasets have been centred to 0‰ by subtracting the error-**
 515 **weighted mean of each dataset. The inset shows the PDF of the inferred age differences between the ice-core data and**
 516 **IntCal13 (green), Lake Suigetsu (yellow) and the Bahamas speleothem (blue). The dashed blue line corresponds to**
 517 **age differences from the modelled mixed layer $\Delta^{14}\text{C}$ and the Bahamas speleothem.**

518

519 Synchronizing the ice-core stack to the speleothem, Lake Suigetsu, and IntCal13 data yields significantly
 520 different results. We infer that GICC05 produces ages about 250 years younger than the U/Th dated speleothem
 521 data (Fig. 10). The IntCal13 record however, implies a larger difference of ~1,000 years. Using Lake Suigetsu
 522 data, on the other hand, leads to multiple probability peaks of which two are in agreement with the speleothem,
 523 and one with the IntCal13 record. The large scatter of the Lake Suigetsu data however, leads to poor statistics
 524 (low χ^2 probabilities). Furthermore, the Lake Suigetsu timescale is only constrained by varve counting back to



525 39 ka BP and based on extrapolation for older sections (Bronk Ramsey et al., 2012) and hence, provides less
526 precise constraints on the timing of the $\Delta^{14}\text{C}$ increase.
527 To test which of these links is the most likely we turn to independent radiometric ages of the Laschamp
528 excursion. Pooled Ar-Ar, K-Ar, and U/Th ages on lava flows place the period of (nearly) reversed field direction
529 at $40,700 \pm 950$ yr BP (Singer et al., 2009), or $41,300 \pm 600$ yr BP (Laj et al., 2014). In addition, a North
530 American speleothem provides a U/Th-dated transient evolution of the geomagnetic field (Lascu et al., 2016),
531 with the lowest intensities occurring at $41,100 \pm 350$ yr BP. Comparing the ice-core ^{10}Be stack to these data
532 clearly shows that all of these records rule out the +1,000 year time shift implied by IntCal13, as it would induce
533 a significant disagreement between radiometrically dated magnetic field records and the dating of the ^{10}Be peak
534 in the ice cores (Fig. 11). We hence argue that the 252 yr offset inferred from the comparison to the Bahamas
535 speleothem is the most likely estimate of the timescale difference between GICC05 and the U/Th timescale
536 around this time. Similar as before, assuming that the speleothem represents a mixed-layer signal instead of
537 direct atmospheric $\Delta^{14}\text{C}$ does not significantly affect the inferred timescale differences (see Fig. 11 inset, blue
538 dashed line).
539



540
541 **Figure 11:** Comparison of the ice-core stack (blue) to Ar-Ar dates of the Laschamp excursion (yellow: Singer et al.
542 2009, pink: Laj et al. 2014), and relative geomagnetic field intensity (black, NRM/ARM, reversed y-axis) from a
543 U/Th-dated speleothem (Lascu et al., 2016). The individual speleothem U/Th dates are shown on the bottom of the
544 figure with their $\pm 2\sigma$ uncertainties. Each panel shows a different shift of GICC05 according to the results from figure
545 10.

546

547 **4.4 Transfer Function**

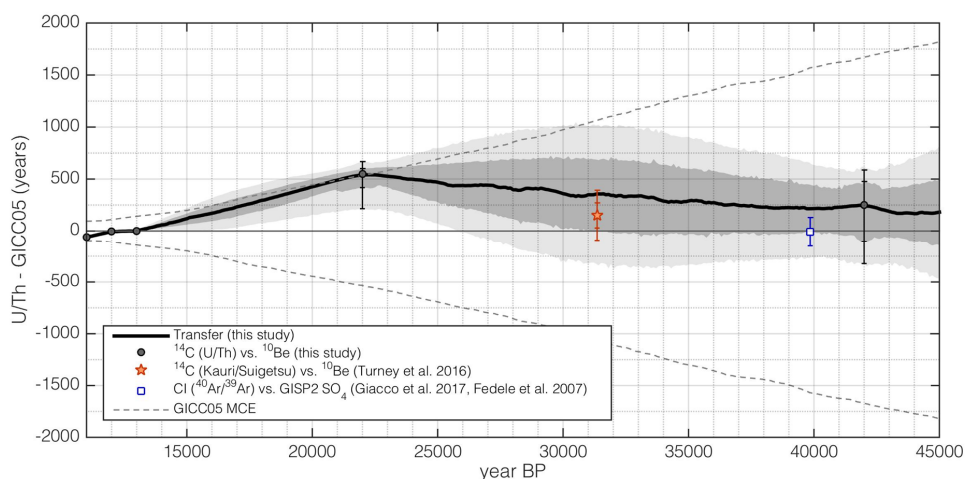
548 To construct a continuous transfer function between GICC05 and the U/Th timescale we apply a Monte-Carlo
549 approach. We randomly sample the PDFs of the timescale differences for each tie-point established in the
550 previous sections (Fig. 7, 9, 10). For the interpolation in-between and the corresponding uncertainties we consult
551 the GICC05 maximum counting error (mce). Since the layer counting uncertainty is incremental, we use the
552 time derivative of the mce to estimate interpolation uncertainty. We generate AR(1) noise ($\mu = 0$, $\sigma = 1$),
553 multiply it with the derivative of the mce, and calculate the cumulative sum back in time. As shown during the
554 Holocene (Adolphi and Muscheler, 2016), the mce is not a random uncorrelated Gaussian error, but appears to
555 be systematic. Hence, we use an AR-process with a strong autocorrelation. We note that this treatment of the
556 mce leads to larger interpolation errors compared to assuming a white noise model, which would lead to very
557 small uncertainties that average out over long time (see also discussion in Rasmussen et al., 2006). Furthermore,
558 we treat the mce as $\pm 1\sigma$ instead of $\pm 2\sigma$ as proposed by Andersen et al. (2006) which additionally increases our
559 interpolation error. We note that this procedure does not aim to provide a realistic model of the ice-core layer-
560 counting process and its uncertainty which is clearly more complex (see Andersen et al., 2006; Rasmussen et al.,
561 2006), nor should it be interpreted such that the mce was a 1σ uncertainty. However, our approach allows us to
562 infer a conservative estimate of the interpolation uncertainty while at the same time it takes advantage of the fact
563 that GICC05 is a layer counted timescale and hence, cannot be stretched/compressed outside realistic bounds.
564 The resulting realizations of the AR(1) process are then used to interpolate between the tie-points established
565 from sampling the PDFs of the $^{14}\text{C}/^{10}\text{Be}$ matches. This procedure was repeated 300,000 times which was found
566 sufficient to obtain a stationary solution, leading to 300,000 possible timescale transfer functions.

567 Figure 12 shows the resulting mean transfer function along with its confidence intervals. Firstly, it can be seen
568 that all tie-points fall into the uncertainty envelope of GICC05. The implied change in the timescale difference
569 between the youngest two tie-points (i.e., over the course of GS-1), and between 13,000 and 22,000 years BP is
570 slightly larger than allowed by the mce, albeit the latter is consistent within the uncertainties of the tie-point at
571 22,000 years BP. We can see that the use of the mce to determine the interpolation error leads to small
572 uncertainties wherever the change in the timescale difference is large (e.g. over the 13,000 – 22,000 years BP
573 interval): Stretching GICC05 by as much as the counting error allows, requires that every uncertain layer has in
574 fact been a real annual layer, leaving little room for additional error. Between 22,000 and 42,000 years BP, the
575 interpolation uncertainties are determined by the mce and thus, grow/shrink at a rate determined by the mce.

576 Our results are in very good agreement with the results by Turney et al. (2016) around Heinrich 3. In this study,
577 a kauri-tree ^{14}C sequence was calibrated onto Lake Suigetsu ^{14}C and also matched on GICC05 via ^{10}Be . The
578 difference of the inferred ages (i.e., kauri on Suigetsu vs. Kauri on GICC05) matches with our proposed transfer
579 function (red star in Fig. 12).

580 Figure 12 also shows the inferred offset between the $^{40}\text{Ar}/^{39}\text{Ar}$ -age of the Campanian Ignimbrite (Giaccio et al.,
581 2017) and a tentatively attributed SO_4 -spike in the GISP2 ice core (Fedele et al., 2007). Even though it
582 obviously requires a well-characterized tephra find in the ice cores to ensure that the SO_4 -peak is indeed
583 associated with the Campanian Ignimbrite, at least from a chronological point of view, our transfer function
584 does not preclude this link. However, no matching shards were identified in this period (Bourne et al., 2013).

585

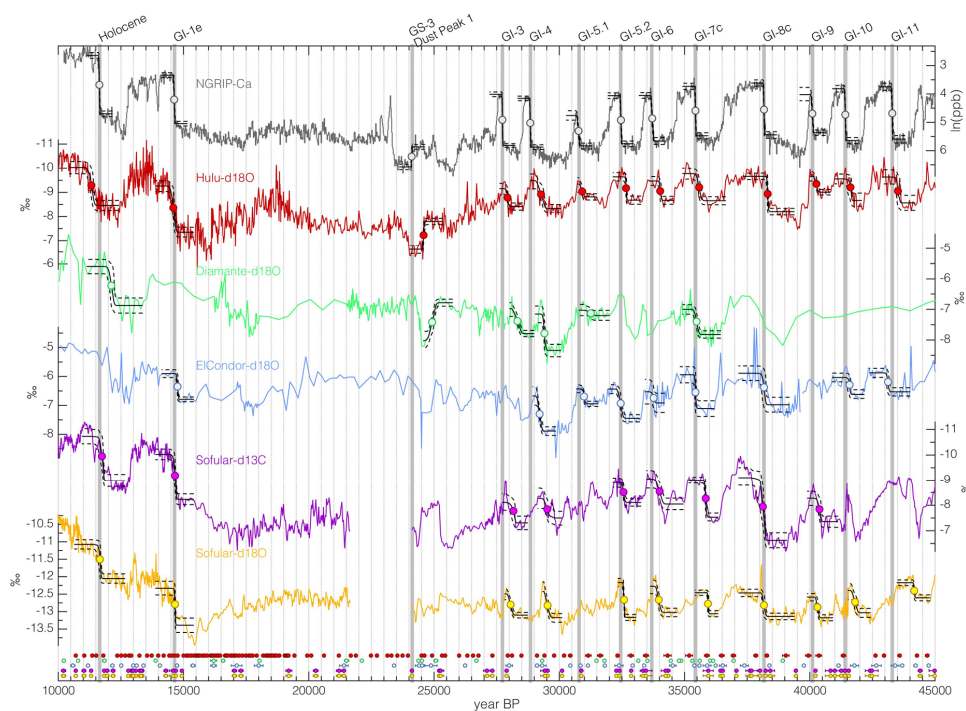


586

587 **Figure 12: Transfer function between the U/Th timescale and GICC05. The transfer function is shown in black with**
588 **dark and light grey shading encompassing its 68.2% and 95.4% confidence intervals. The black dots with error bars**
589 **show the used match points between ^{14}C and ^{10}Be . The red star shows the difference between ages of a glacial kauri**
590 **tree ^{14}C sequence on Lake Suigetsu ^{14}C and GRIP ^{10}Be (Turney et al., 2016). The blue open square shows the age**
591 **difference between the $^{40}\text{Ar}/^{39}\text{Ar}$ -age of the Campanian Ignimbrite (Giaccio et al., 2017), and a tentatively associated**
592 **spike in the GISP2 SO_4 record (Fedele et al., 2007) on the GICC05 timescale (Seierstad et al., 2014).**

593 5 The timing of DO-events

594 To investigate the synchronicity of climate changes recorded in different parts of the globe, we compare ice-core
595 data to a selection of well-dated speleothem records. The well-known Hulu-Dongge Cave records have become
596 iconic blueprints for intensity changes of the East Asian Summer Monsoon (EASM) anchored on a precise U/Th
597 timescale (Cheng et al., 2016; Dykoski et al., 2005; Wang et al., 2001). The speleothem records from Cueva del
598 Diamante and El Condor reflect changes in precipitation amount over eastern Amazonia associated with the
599 South American Monsoon (Cheng et al., 2013b). The speleothem records from Sofular Cave, Turkey, are not
600 straightforward in their mechanistic interpretation but likely reflect a mix of temperature and seasonality of
601 precipitation ($\delta^{18}\text{O}$), and type and density of vegetation, soil microbial activity ($\delta^{13}\text{C}$), and hence, effective
602 moisture and temperature (Fleitmann et al., 2009). Hence, while this list of speleothem data can certainly be
603 expanded in future studies, we chose these four speleothem records from 3 different regions that are all well-
604 dated and sensitive to the position of the ITCZ and compare it to the ice-core records.



605

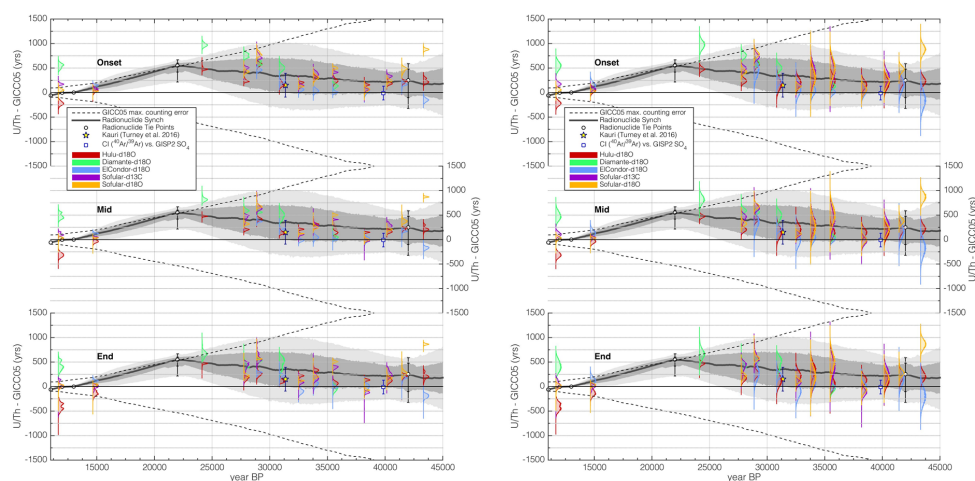
606 **Figure 13: Timing of abrupt climate changes in different climate records. The climate archive and proxy is indicated**
607 **in each panel. The black lines show the mean of the fitted ramps and their 95% confidence intervals (dashed). The**
608 **dots mark the midpoint of the mean transition. The U/Th dates and their $\pm 1\sigma$ uncertainties of each climate record are**
609 **shown at the bottom of the figure in colour coding corresponding to the respective climate record. Each time series is**
610 **shown on its original timescale not applying any synchronization.**

611

612 Figure 13 shows the ice-core and speleothem climate records on their original individual timescales, along with
613 the fitted ramps to the rapid climate changes. Note that we could not fit each climate event for every record,
614 since the method requires a minimum number of data points defining the levels before and after each transition
615 to produce reliable estimates. Already visually, a lag of climate changes in Greenland compared to the
616 speleothem records can be consistently identified between 20 and 35 ka BP when all records are on their
617 original timescales. Combining the PDFs of the detected change points in Greenland and the speleothems allows
618 us to infer a probability estimate of the timing difference between climate events in Greenland and speleothems.
619 These differences are shown in figure 14 along with our transfer function based on the matching of
620 radionuclides from figure 12. This comparison shows that the differences in the timing of start-, mid- and end-
621 point of DO-events in speleothems and ice cores largely fall within the uncertainties of our radionuclide-based
622 timescale transfer function. Thus, rapid climate changes occur synchronously in Greenland and the (sub-)
623 tropics. Notable exceptions are i) the transition from GS-1 to the Holocene around 11.6 ka BP, ii) Heinrich event
624 2 at 24 ka BP, and iii) DO-11 around 43 ka BP. However, there is large scatter among the different speleothem-
625 based estimates at these events, indicating that these events are asynchronous in the different speleothems
626 records on their respective timescales. Consequently, some of these records also imply asynchronous climate
627 shifts with Greenland ice cores. This may either be interpreted as an indication of time-transgressive climate



628 changes, or as a bias in individual speleothems – either in how climate is recorded in the speleothem, or their
 629 dating (for example through detrital thorium).



630 **Figure 14: Timing differences of the onset (top), midpoint (middle) and end (bottom) of rapid climate changes in**
 631 **NGRIP and speleothems (coloured PDFs, see legend), and the timescale transfer function inferred from radiocarbon**
 632 **matching (black line and grey shadings as in figure 12). The left panels show the PDFs of timing differences including**
 633 **only uncertainties from the determination of the change points in the climate records, while the right hand panels**
 634 **also include the speleothem dating uncertainties.**

635

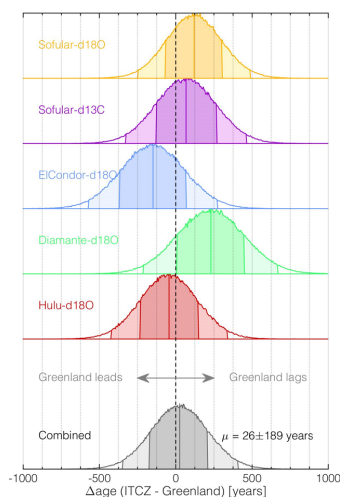
636 Averaging over all DO events, we can estimate an overall probability of leads and lags. By using the individual
 637 realizations of the radionuclide-based transfer function (see section 4.4) we take into account that the
 638 uncertainties of the transfer function are strongly autocorrelated. For each realization, we randomly sample the
 639 PDFs for the onset of the DO-events for the ice-core and speleothem records, perturb the speleothem-based
 640 estimates within their U/Th dating errors, determine the lead or lag between the DO-onset in ice-core and
 641 speleothem records, and correct it for the expected lag from the realization of our transfer function. By
 642 averaging over all DO-events we thus obtain a mean lag for each realization and speleothem. In addition, we
 643 combine the different speleothem-based estimates of each realization by averaging over their mean lags to
 644 obtain an overall (speleothem & DO-event) mean lag. Converting the obtained lags from each realization into
 645 histograms we estimate the PDFs of average lags between ice-core and speleothem records.

646 Our lag estimates critically depend on our ability to fill the gaps between the widely spaced tie-points and thus,
 647 on our assumptions about the ice-core layer counting uncertainty, and how well our AR(1) process model can
 648 capture these (section 4). However, we note that by treating the mce as a highly correlated 1σ (instead of 2σ)
 649 uncertainty, our error estimate can be regarded as very conservative since it allows for large systematic drifts in
 650 each realization of the transfer function that will result in large errors of the mean.

651 The resulting PDFs of the lag between speleothems and ice cores are shown in figure 15. The uncertainties are
 652 mainly determined by our synchronization uncertainty. Thus, the uncertainty is only marginally reduced when
 653 averaging over all speleothems (Fig. 15, bottom): Because each realization of the transfer function varies
 654 smoothly, the offset between speleothem and ice-core records will be systematic for all speleothems in each
 655 realization, and is thus only marginally reduced by averaging.



656 We find that all speleothem records except Cueva del Diamante (Cheng et al., 2013b) indicate synchronicity
 657 with NGRIP within 1σ and that the delay obtained for Cueva del Diamante falls within 2σ . We note that the
 658 speleothem data from El Condor (Cheng et al., 2013b) from the same region as Cueva del Diamante does not
 659 indicate a significant lag to Greenland. Overall, our analysis cannot reject the null-hypothesis of synchronous
 660 DO-events in Greenland ice cores and (sub-) tropical speleothems (lag: $\mu \pm 1\sigma = 29 \pm 189$ years).



661

662 **Figure 15:** Average lead/lag between the onset of DO-events in the speleothems and NGRIP. Each panel (colour)
 663 shows the PDF for the lead/lag of the onset in the speleothem compared to NGRIP, averaged over all investigated
 664 DO-events (i.e., excluding the GS-3 Dust Peak/H2). The bottom most panel shows the PDF of the average of all DO-
 665 events and speleothems. The dark/light shading of the PDF in each panel indicates 68.2%/95.4% intervals.

666 6 Discussion

667 Our proposed transfer function quantifies the long-term differences between the Greenland ice-core and U/Th
 668 timescale and allows their synchronization. Even though based on only a few tie-points, this can be used to
 669 evaluate the absolute dating accuracy of Greenland ice-core records during the past 45 ka BP, while maintaining
 670 the strength of their precise relative dating. In combination with similar work done for the Holocene (Adolphi
 671 and Muscheler, 2016; Muscheler et al., 2014a), the picture emerges that the GICC05 counting error may be
 672 systematic: when accumulation and data resolution is high (e.g. in parts of the Holocene), too many annual
 673 layers have been counted, whereas during periods of low accumulation (e.g. GS-1 and GS-2) there is a tendency
 674 to identify too few annual layers. In principle, this is well captured by the GICC05 uncertainty estimate as the
 675 derivative of our transfer function is (within error) consistent with the increase of the counting error. However,
 676 our results caution against the use of the GICC05 counting error as a 2σ uncertainty as is often done in the
 677 literature. Originally, Andersen et al. (2006) pointed out that the MCE is not a true σ uncertainty but proposed
 678 that a Gaussian distribution with $2\sigma = \text{MCE}$ could serve as a pragmatic approximation. In combination with
 679 results from the Holocene (Adolphi and Muscheler, 2016) our study shows that the counting error can be
 680 strongly correlated over extended periods of time. This is in line with the discussion in Rasmussen et al. (2006)
 681 who point out that the main contribution to a potential bias in the layer count is the definition of how an annual
 682 layer is manifested in the proxy data. The data resolution as well as the manifestation of annual layers change



683 between different climate states (Rasmussen et al., 2006), likely due to changes in aerosol transport and
684 deposition resulting from variations in the atmospheric circulation and seasonality of precipitation (Merz et al.,
685 2013; Werner et al., 2001). According to our analysis, the largest relative (i.e., year/year) change in the
686 difference between GICC05 and the U/Th and tree-ring timescale occurs over GS-1 (11,653-12,846 years BP)
687 and GS-2 (14,652-23,290 years BP). Both of these periods have likely been characterized by an increased
688 relative contribution of summer precipitation to the annual ice layer (Werner et al., 2000; Denton et al., 2005),
689 and the annual layers in the ice core have been identified in a similar way in both intervals (Rasmussen et al.,
690 2006). In the 11-13 ka BP interval, the offset between GICC05 and the tree-ring timescale changes from -60
691 (95.4%-range: -77 to -42) years to zero (95.4%-range: -12 to +21) years. During the same interval, the GICC05
692 maximum counting error grows by 46 years. Albeit consistent within the absolute error margins, this stretch of
693 GICC05 over GS-1 thus slightly exceeds the range allowed by the GICC05 counting error. Muscheler et al.
694 (2014a) discussed that this stretch may be partly explained by errors in the placement of the oldest part of the
695 tree-ring chronologies. However, here, we use a revised late glacial tree-ring dataset in which the different
696 chronologies are connected much more robustly (Hogg et al., 2016). Furthermore, our analysis on the fully
697 independent Hulu Cave ^{14}C data yields similar results (Fig. 7). Hence, our analyses clearly show that the GS-1
698 interval is about 60 years too short in the GICC05-timescale.

699 Between 15 and 22 ka BP, our analysis yields a change in the GICC05 offset from +118 (95.4%-range: 2-220)
700 years to +549 (95.4%-range: 207-670) years, while the GICC05 counting error grows by 335 years. Thus, again,
701 our transfer function changes a little faster than the maximum counting error allows during this interval. We
702 note that our ^{14}C - ^{10}Be matchpoint around 22,000 years BP has a relatively low signal-to-noise ratio in the ^{14}C
703 data (see Fig. 8-9) and should, thus, be regarded as tentative. However, as shown in figure 8 our results are
704 generally robust against different choices of subsets of the ^{14}C data and time windows. Nevertheless, it can also
705 be seen that the estimates of the most likely age difference (i.e., the peak of the PDFs) differ slightly for
706 different choices of the ^{14}C data. Hulu Cave yields a most likely offset of ~325 years, while Suigetsu implies a
707 bigger age difference of ~550 years that coincides with a secondary probability peak in the Hulu Cave PDF. We
708 note that assuming increased amounts of old soil organic carbon contributing to the speleothem formation would
709 lead to an even stronger difference between these estimates (see section 3.4). Hence, we propose an age
710 difference of +549 (95.4% range: 207-670) years based on the combination of all data (Fig. 9) that is consistent
711 within error with the estimates based on the single datasets shown in figure 8, but stress that this tie-point should
712 be re-evaluated as new suitable ^{14}C data becomes available in the future.

713 Assuming that the U/Th dates are absolute, our transfer function can be used to account for the bias in the
714 GICC05 timescale and thus facilitate comparisons of ice-core records to other absolutely dated archives.
715 However, we note that our synchronization does not necessarily lead to consistent timescales with radiocarbon-
716 dated records. As discussed in section 3.3.2 (Fig. 4) and section 4.3 (Fig. 10 & 11), discrepancies of the datasets
717 underlying IntCal13 can lead to erroneous structures in the calibration curve. The reduced amplitude of the $\Delta^{14}\text{C}$
718 change around the Laschamp geomagnetic field minimum in IntCal13 compared to its underlying data implies
719 that IntCal $\Delta^{14}\text{C}$ must be offset prior to and/or after the Laschamp event. This underlines the challenges in
720 radiocarbon calibration around this time pointed out by Muscheler et al. (2014b). Also more recently, Giaccio et
721 al. (2017) pointed out that paired $^{40}\text{Ar}/^{39}\text{Ar}$ and ^{14}C -dating of the Campanian Ignimbrite around 40 ka BP yields
722 inconsistent ages when the ^{14}C age is calibrated with IntCal13. Since IntCal13 in principle should be tied to the



723 U/Th-age scale, this implies either an inconsistency between Ar/Ar and U/Th dating or in the reconstructed ^{14}C
724 levels of the calibration curve. The latter would be congruent with the conclusions by Muscheler et al. (2014b).
725 If the problem was indeed the IntCal ^{14}C reconstruction, a synchronization of ice-core ^{10}Be to IntCal ^{14}C would
726 not resolve this bias, since the problem would not be one of chronology, but of ^{14}C measurement and/or archive.
727 Our analysis provides the first rigorous test of whether DO-events recorded in speleothems and ice cores occur
728 synchronously. We find that on average, the onset of DO-events occurs simultaneously within the precision of
729 our method ($\pm 1\sigma = \pm 189$ years), consistent with the findings of Baumgartner et al. (2014). Since we compare to
730 speleothem records from different regions, this also highlights that the ITCZ likely migrated synchronously
731 (within uncertainties) over the different ocean basins and continents during the onset of DO-events. However,
732 there are also differences between the different speleothem records, which could be due to limitations in their
733 dating or related to how directly individual archives record the rapid climate changes. The most notable
734 examples are the onset of the Holocene and GI-11, which appear to occur asynchronously in the different
735 speleothems (see Fig. 13 & 14). Another example is the younger GS-3 dust peak in the Greenland ice cores that
736 appears to coincide with the East Asian Summer Monsoon decline seen in Hulu Cave, but postdates the
737 precipitation increase seen in El Condor and Diamante. This change in the speleothems is typically attributed to
738 the southward shift of the ITCZ as a response to Heinrich Event 2.

739 Figure 16 shows the period around H2. Firstly, we note that the younger of the two GS-3 dust peaks in the
740 Greenland ice cores (Rasmussen et al., 2014a) occurs coevally (within chronological uncertainty) with the ITCZ
741 movement recorded by the speleothems. At this time, the East Asian Summer Monsoon is strongly reduced as
742 implied by decreased Hulu Cave $\delta^{18}\text{O}$ (Cheng et al., 2016). Coevally, precipitation increases in the South
743 American Summer Monsoon region (Novello et al., 2017; Stríkis et al., 2018). The records thus exhibit more
744 pronounced stadial conditions than normally seen during (non-Heinrich) DO-events. However, taken at face
745 value, the precipitation increase at El Condor and Cueva del Diamante, the two northernmost sites shown in
746 figure 16 (Cheng et al., 2013b), significantly predates the event seen in Greenland and Hulu Cave. It also
747 predates the more southern South American sites Lapa Sem Fim (Stríkis et al., 2018) and Jaragua (Novello et
748 al., 2017) by more than 500 years. This could either point to errors in the dating of the El Condor and Diamante
749 speleothems, or be related to their latitudinal position. A freshwater-only experiment (all other boundary
750 conditions held constant at 19 ka BP levels) with the Community Climate System Model 3 (TraCE-MWF, He,
751 2011) shows that, during a weak AMOC state, reduced advection of moisture from the tropical Atlantic leads to
752 lower precipitation north of the ITCZ (Fig. 16). El Condor and Cueva del Diamante are both located very close
753 to the LGM position of the ITCZ. It is hence possible, that when northern hemisphere summer insolation
754 reached its lowest values over the past 50 kaBP around H2, the ITCZ migrated to a position south of El Condor
755 and Cueva del Diamante. As a result, the precipitation response to freshwater forcing would change sign at these
756 cave sites. The sites located slightly further south only show a weak (Pacupahuain) or no (Paixao) response
757 during this period, but are both characterized by increased variability. The two southernmost sites on the other
758 hand (Jaragua and Lapa Sem Fim) remain south of the ITCZ throughout, and hence, show a clear increase in
759 precipitation coeval with the signal in Greenland and Hulu Cave. In this context, the precipitation increase in El
760 Condor and Cueva del Diamante around 25kaBP (i.e., prior to H2) may signify when the ITCZ transitions over
761 the sites. The subsequent reduction in AMOC strength during H2 then leads to a decrease in precipitation in
762 north-west South America, an increase further south, and little change in between. Tentative support for this can



763 be drawn from the response of the El Condor and Cueva del Diamante speleothems to GI-2.2 and GI-2.1 where,
 764 albeit weakly, the $\delta^{18}\text{O}$ records imply an increase in precipitation during GI-2 which is opposite to their
 765 response to DO-events during MIS-3 (Fig. 13, 16). Thus, this analysis indicates, that the seemingly
 766 asynchronous response to climate change in different proxy records may indeed only reflect site specific
 767 changes in the proxy response. Alternatively, we cannot rule out undetected issues with the U/Th ages of these
 768 speleothems. A detailed analysis of this observation feature is beyond the scope of this paper, but in the context
 769 of a timescale perspective, which is the focus of this work, it highlights the caveats of climate wiggle-matching
 770 between single records, even if the mechanistic link between regional climate changes may be relatively well
 771 understood.

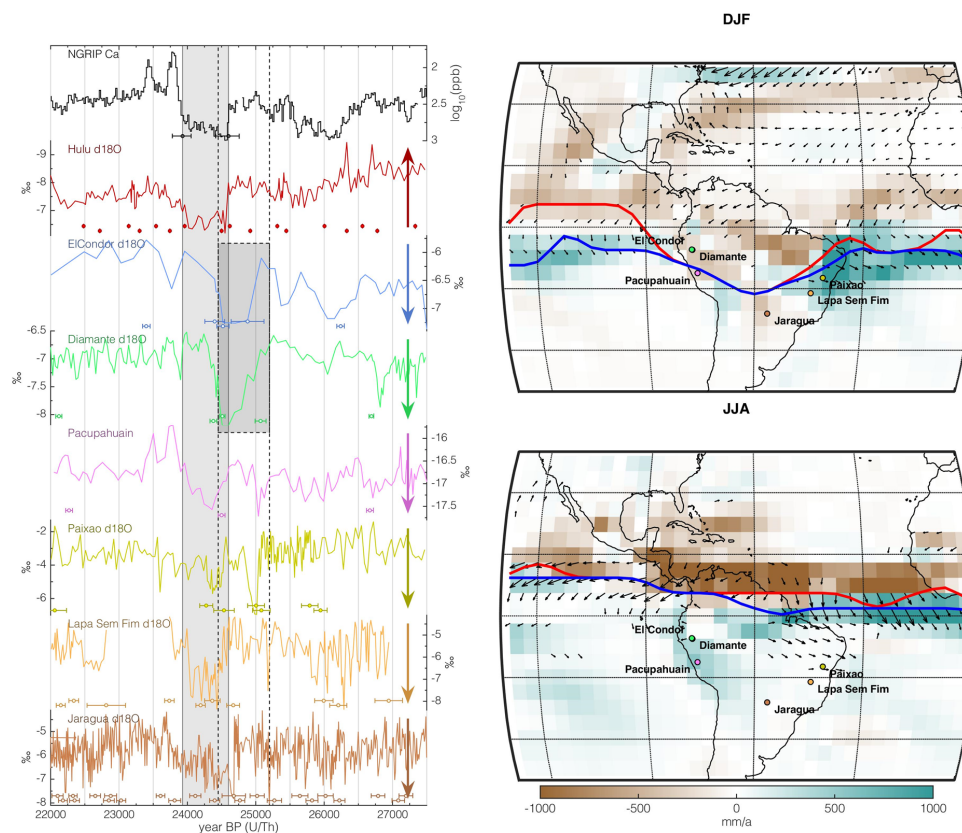


Figure 16: Climate changes around H2. Left (from top to bottom): NGRIP Ca (Bigler, 2004) on the synchronized timescale (Fig. 14), Hulu Cave $\delta^{18}\text{O}$ (Cheng et al., 2016), El Condor $\delta^{18}\text{O}$ (Cheng et al., 2013b), Cueva del Diamante $\delta^{18}\text{O}$ (Cheng et al., 2013b), Pacupahuain $\delta^{18}\text{O}$ (Kanner et al., 2012), Paixao $\delta^{18}\text{O}$ (Strikis et al., 2018), Lapa Sem Fim $\delta^{18}\text{O}$ (Strikis et al., 2018), Jaragua Cave $\delta^{18}\text{O}$ (Novello et al., 2017). The arrows on the right hand side of each axis point in the direction of the signature of increased precipitation on $\delta^{18}\text{O}$ through the amount effect (Dansgaard, 1964). The light grey box marks H2. The dark grey box highlights the preceding $\delta^{18}\text{O}$ anomaly in El Condor and Diamante caves. Right: Precipitation (colour) and wind (arrows) response to freshwater forcing in the CCSM3 climate model (freshwater only experiment of TraCE21k, all other forcings are held at 19k conditions, He, 2011). The red (blue) line depicts the latitude of the precipitation maximum during strong (weak) AMOC-states. Only wind anomalies $>1\text{m/s}$ are plotted. The top panel shows the winter (December-February) response, while the bottom panel shows the summer (June-August) response. Anomalies are plotted as weak-strong AMOC mode.



772

773 **7 Conclusion**

774 We present the first radionuclide-based comparison between the Greenland Ice Core Chronology 2005
775 (GICC05) and the U/Th timescale. We find that GICC05 is accurate within its stated absolute uncertainties, but
776 also that the maximum counting error of the GICC05 may be at the limit to capture the total uncertainty
777 accumulated within certain climatic periods. Our analysis indicates that the relationship between GICC05 and
778 the U/Th timescale over the last 45 ka drifts over time and reaches its maximum offset around 22 ka BP. We
779 propose a transfer function that quantifies this drift and facilitates analysis of ice-core and U/Th records, such as
780 speleothems, on a common time scale. Thus, this transfer function allows further integration of key-timescales
781 in paleosciences and contributes to the INTIMATE (INTEgration of Ice-core, MARine, and TEerrestrial records)
782 initiative (Björck et al., 1996; Rasmussen et al., 2014b; Bronk Ramsey et al., 2014). Provided that U/Th ages are
783 regarded accurate, the transfer function reduces the absolute dating uncertainty of Greenland ice cores by 50-
784 70% back to 45 ka BP. We find that, on average, the onset of DO-events occurs synchronously in Greenland,
785 East Asia, and South America. We show that the southward ITCZ shift around 24.5 ka BP seen in speleothems,
786 typically associated with H2, coincides with the younger GS-3 dust peak recorded in Greenland ice cores.
787 However, we also highlight inconsistencies between speleothem records around the onset of the Holocene, late
788 GS-3, and GI-11 and thus, caveats to the commonly applied practice of climate wiggle-matching.
789 By comparing various ^{14}C records underlying IntCal13 as well as ice-core ^{10}Be data and geomagnetic field
790 records, we infer that the current radiocarbon calibration curve underestimates the amplitude and rapidity of the
791 $\Delta^{14}\text{C}$ change around the Laschamp event 41 ka BP. This adds to previous studies (Giaccio et al., 2017;
792 Muscheler et al., 2014b) highlighting that there are likely systematic errors in IntCal13 that will directly
793 translate into errors of radiocarbon-based chronologies around that time. The combination of several internally
794 inconsistent datasets in IntCal13 can lead to erroneous timing and amplitude of $\Delta^{14}\text{C}$ changes. Hence, great care
795 has to be taken when attempting to use sections older than 30 ka BP of IntCal13 directly for studies of ^{14}C
796 production rates and/or carbon cycle changes.

797 **8 Data Availability**

798 The transfer function shown in figure 12 will be made available as a supplementary to this paper and on NOAA.

799 **9 Author contributions**

800 FA designed and carried out analyses, and wrote the manuscript in correspondence with CBR and RM. TE
801 designed and applied break-point detection analysis and wrote the corresponding methods section. FA, RM,
802 CBR, SOR, CT and AC initiated the project. RLE and HC provided speleothem data. AS and SOR provided
803 insights into the ice core chronology. HF and TE gave insights into aerosol transport and deposition. All authors
804 discussed and commented on the manuscript.



805 **10 Competing interests**

806 The authors declare that they have no conflict of interest.

807

808 **11 Acknowledgements**

809 FA was supported through a grant by the Swedish Research Council to FA (Vetenskapsrådet DNr. 2016-00218).
810 CBR was partially supported through the UK Natural Environment Research Council (NERC) Radiocarbon
811 Facility (NRCF010002). TE and HF acknowledge the long-term support of ice-core research at the University of
812 Bern by the Swiss National Science Foundation (SNSF) and the Oeschger Center for Climate Change Research.
813 SOR gratefully acknowledges support from the Carlsberg Foundation to the project ChronoClimate. This work
814 was partially supported by the Swedish Research Council (grant DNR2013-8421 to RM), the NSF 1702816 to
815 RLE, and the Australian Research Council DPI70104665 to CT and AC. We gratefully acknowledge the
816 financial support of the University of Adelaide Environment Institute, for the initial Marble Hill meeting that
817 initiated this work.

818 **References**

819 Adolphi, F., Muscheler, R., Svensson, A., Aldahan, A., Possnert, G., Beer, J., Sjolte, J., Björck, S.,
820 Matthes, K., and Thiéblemont, R.: Persistent link between solar activity and Greenland climate
821 during the Last Glacial Maximum, *Nat Geosci*, 7, 662-666, 10.1038/ngeo2225, 2014.

822 Adolphi, F., and Muscheler, R.: Synchronizing the Greenland ice core and radiocarbon timescales
823 over the Holocene – Bayesian wiggle-matching of cosmogenic radionuclide records, *Clim. Past*, 12,
824 15-30, 10.5194/cp-12-15-2016, 2016.

825 Adolphi, F., Muscheler, R., Friedrich, M., Güttler, D., Wacker, L., Talamo, S., and Kromer, B.:
826 Radiocarbon calibration uncertainties during the last deglaciation: Insights from new floating tree-
827 ring chronologies, *Quaternary Sci Rev*, 170, 98-108,
828 <https://doi.org/10.1016/j.quascirev.2017.06.026>, 2017.

829 Andersen, K. K., Svensson, A., Johnsen, S. J., Rasmussen, S. O., Bigler, M., Röthlisberger, R., Ruth, U.,
830 Siggaard-Andersen, M.-L., Peder Steffensen, J., and Dahl-Jensen, D.: The Greenland Ice Core
831 Chronology 2005, 15–42ka. Part 1: constructing the time scale, *Quaternary Sci Rev*, 25, 3246-3257,
832 10.1016/j.quascirev.2006.08.002, 2006.

833 Bard, E., Raisbeck, G. M., Yiou, F., and Jouzel, J.: Solar modulation of cosmogenic nuclide production
834 over the last millennium: comparison between ¹⁴C and ¹⁰Be records, *Eart Planet Sc Lett*, 150, 453-
835 462, 10.1016/s0012-821x(97)00082-4, 1997.

836 Bard, E., Arnold, M., Hamelin, B., Tisnerat-Laborde, N., and Cabioch, G.: Radiocarbon Calibration by
837 Means of Mass Spectrometric ²³⁰Th/²³⁴U and ¹⁴C Ages of Corals: An Updated Database Including
838 Samples from Barbados, Mururoa and Tahiti, *Radiocarbon*, 40, 1085-1092,
839 10.1017/S0033822200019135, 1998.



- 840 Bard, E., Ménot, G., Rostek, F., Licari, L., Böning, P., Edwards, R. L., Cheng, H., Wang, Y., and Heaton,
841 T. J.: Radiocarbon calibration/comparison records based on marine sediments from the Pakistan and
842 Iberian margins, *Radiocarbon*, 55, 1999-2019, 2013.
- 843 Baumgartner, M., Kindler, P., Eicher, O., Floch, G., Schilt, A., Schwander, J., Spahni, R., Capron, E.,
844 Chappellaz, J., Leuenberger, M., Fischer, H., and Stocker, T. F.: NGRIP CH₄ concentration from 120 to
845 10 kyr before present and its relation to a $\delta^{15}\text{N}$ temperature reconstruction from the same ice core,
846 *Clim. Past*, 10, 903-920, 10.5194/cp-10-903-2014, 2014.
- 847 Baumgartner, S., Beer, J., Suter, M., Dittrich-Hannen, B., Synal, H. A., Kubik, P. W., Hammer, C., and
848 Johnsen, S.: Chlorine 36 fallout in the Summit Greenland Ice Core Project ice core, *Journal of*
849 *Geophysical Research: Oceans*, 102, 26659-26662, 10.1029/97JC00166, 1997a.
- 850 Baumgartner, S., Beer, J., Wagner, G., Kubik, P., Suter, M., Raisbeck, G. M., and Yiou, F.: ¹⁰Be and
851 dust, Nuclear Instruments and Methods in Physics Research Section B: Beam Interactions with
852 Materials and Atoms, 123, 296-301, 10.1016/S0168-583X(96)00751-3, 1997b.
- 853 Baumgartner, S., Beer, J., Masarik, J., Wagner, G., Meynadier, L., and Synal, H.-A.: Geomagnetic
854 Modulation of the ³⁶Cl Flux in the GRIP Ice Core, Greenland, *Science*, 279, 1330-1332,
855 10.1126/science.279.5355.1330, 1998.
- 856 Bigler, M.: Hochauflösende Spurenstoffmessungen an polaren Eisbohrkernen: Glazio-chemische und
857 klimatische Prozessstudien, PhD, Environmental Physics, University of Bern, Bern, 2004.
- 858 Björck, S., Kromer, B., Johnsen, S., Bennike, O., Hammarlund, D., Lemdahl, G., Possnert, G.,
859 Rasmussen, T. L., Wohlfarth, B., Hammer, C. U., and Spurk, M.: Synchronized Terrestrial/Atmospheric
860 Deglacial Records Around the North Atlantic, *Science*, 274, 1155-1160,
861 10.1126/science.274.5290.1155, 1996.
- 862 Bourne, A. J., Davies, S. M., Abbott, P. M., Rasmussen, S. O., Steffensen, J. P., and Svensson, A.:
863 Revisiting the Faroe Marine Ash Zone III in two Greenland ice cores: implications for marine - ice
864 correlations, *Journal of Quaternary Science*, 28, 641-646, doi:10.1002/jqs.2663, 2013.
- 865 Broecker, W. S.: A preliminary evaluation of uranium series inequilibrium as a tool for absolute age
866 measurement on marine carbonates, *J Geophys Res*, 68, 2817-2834, 10.1029/JZ068i009p02817,
867 1963.
- 868 Bronk Ramsey, C., van der Plicht, J., and Weninger, B.: " Wiggle matching" radiocarbon dates,
869 *Radiocarbon*, 43, 381-390, 2001.
- 870 Bronk Ramsey, C., Staff, R. A., Bryant, C. L., Brock, F., Kitagawa, H., van der Plicht, J., Schlolaut, G.,
871 Marshall, M. H., Brauer, A., Lamb, H. F., Payne, R. L., Tarasov, P. E., Haraguchi, T., Gotanda, K.,
872 Yonenobu, H., Yokoyama, Y., Tada, R., and Nakagawa, T.: A complete terrestrial radiocarbon record
873 for 11.2 to 52.8 kyr B.P, *Science*, 338, 370-374, 10.1126/science.1226660, 2012.
- 874 Bronk Ramsey, C., Albert, P., Blockley, S., Hardiman, M., Lane, C., Macleod, A., Matthews, I. P.,
875 Muscheler, R., Palmer, A., and Staff, R. A.: Integrating timescales with time-transfer functions: a



876 practical approach for an INTIMATE database, *Quaternary Sci Rev*, 106, 67-80,
877 [10.1016/j.quascirev.2014.05.028](https://doi.org/10.1016/j.quascirev.2014.05.028), 2014.

878 Buizert, C., Adrian, B., Ahn, J., Albert, M., Alley, R. B., Baggenstos, D., Bauska, T. K., Bay, R. C.,
879 Bencivengo, B. B., Bentley, C. R., Brook, E. J., Chellman, N. J., Clow, G. D., Cole-Dai, J., Conway, H.,
880 Cravens, E., Cuffey, K. M., Dunbar, N. W., Edwards, J. S., Fegyveresi, J. M., Ferris, D. G., Fitzpatrick, J.
881 J., Fudge, T. J., Gibson, C. J., Gkinis, V., Goetz, J. J., Gregory, S., Hargreaves, G. M., Iverson, N.,
882 Johnson, J. A., Jones, T. R., Kalk, M. L., Kippenhan, M. J., Koffman, B. G., Kreutz, K., Kuhl, T. W., Lebar,
883 D. A., Lee, J. E., Marcott, S. A., Markle, B. R., Maselli, O. J., McConnell, J. R., McGwire, K. C., Mitchell,
884 L. E., Mortensen, N. B., Neff, P. D., Nishiizumi, K., Nunn, R. M., Orsi, A. J., Pasteris, D. R., Pedro, J. B.,
885 Pettit, E. C., Price, P. B., Priscu, J. C., Rhodes, R. H., Rosen, J. L., Schauer, A. J., Schoenemann, S. W.,
886 Sendelbach, P. J., Severinghaus, J. P., Shturmakov, A. J., Sigl, M., Slawny, K. R., Souney, J. M., Sowers,
887 T. A., Spencer, M. K., Steig, E. J., Taylor, K. C., Twickler, M. S., Vaughn, B. H., Voigt, D. E., Waddington,
888 E. D., Welten, K. C., Wendricks, A. W., White, J. W. C., Winstrup, M., Wong, G. J., and Woodruff, T. E.:
889 Precise inter polar phasing of abrupt climate change during the last ice age, *Nature*, 520, 661-665,
890 [10.1038/nature14401](https://doi.org/10.1038/nature14401)
891 [http://www.nature.com/nature/journal/v520/n7549/abs/nature14401.html#supplementary-](http://www.nature.com/nature/journal/v520/n7549/abs/nature14401.html#supplementary-information)
892 [information](http://www.nature.com/nature/journal/v520/n7549/abs/nature14401.html#supplementary-information), 2015.

893 Cauquoin, A., Raisbeck, G. M., Jouzel, J., and Paillard, D.: Use of ^{10}Be to Predict Atmospheric ^{14}C
894 Variations during the Laschamp Excursion: High Sensitivity to Cosmogenic Isotope Production
895 Calculations, *Radiocarbon*, 56, 67-82, [10.2458/56.16478](https://doi.org/10.2458/56.16478), 2014.

896 Cheng, H., Lawrence Edwards, R., Shen, C.-C., Polyak, V. J., Asmerom, Y., Woodhead, J., Hellstrom, J.,
897 Wang, Y., Kong, X., Spötl, C., Wang, X., and Calvin Alexander Jr, E.: Improvements in ^{230}Th dating,
898 ^{230}Th and ^{234}U half-life values, and U-Th isotopic measurements by multi-collector inductively
899 coupled plasma mass spectrometry, *Earth Planet Sc Lett*, 371-372, 82-91,
900 [http://dx.doi.org/10.1016/j.epsl.2013.04.006](https://doi.org/10.1016/j.epsl.2013.04.006), 2013a.

901 Cheng, H., Sinha, A., Cruz, F. W., Wang, X., Edwards, R. L., d'Horta, F. M., Ribas, C. C., Vuille, M., Stott,
902 L. D., and Auler, A. S.: Climate change patterns in Amazonia and biodiversity, *Nat Commun*, 4, 1411,
903 [10.1038/ncomms2415](https://doi.org/10.1038/ncomms2415)
904 <https://www.nature.com/articles/ncomms2415#supplementary-information>, 2013b.

905 Cheng, H., Edwards, R. L., Sinha, A., Spötl, C., Yi, L., Chen, S., Kelly, M., Kathayat, G., Wang, X., Li, X.,
906 Kong, X., Wang, Y., Ning, Y., and Zhang, H.: The Asian monsoon over the past 640,000 years and ice
907 age terminations, *Nature*, 534, 640-646, [10.1038/nature18591](https://doi.org/10.1038/nature18591)
908 [http://www.nature.com/nature/journal/v534/n7609/abs/nature18591.html#supplementary-](http://www.nature.com/nature/journal/v534/n7609/abs/nature18591.html#supplementary-information)
909 [information](http://www.nature.com/nature/journal/v534/n7609/abs/nature18591.html#supplementary-information), 2016.

910 Craig, H.: The Natural Distribution of Radiocarbon and the Exchange Time of Carbon Dioxide
911 Between Atmosphere and Sea, *Tellus*, 9, 1-17, [10.1111/j.2153-3490.1957.tb01848.x](https://doi.org/10.1111/j.2153-3490.1957.tb01848.x), 1957.

912 Cutler, K., Gray, S., Burr, G., Edwards, R., Taylor, F., Cabioch, G., Beck, J., Cheng, H., and Moore, J.:
913 Radiocarbon calibration and comparison to 50 kyr BP with paired ^{14}C and ^{230}Th dating of corals
914 from Vanuatu and Papua New Guinea, *Radiocarbon*, 46, 1127-1160, 2004.

915 Dansgaard, W.: Stable isotopes in precipitation, *Tellus*, 16, 436-468, [doi:10.1111/j.2153-](https://doi.org/10.1111/j.2153-3490.1964.tb00181.x)
916 [3490.1964.tb00181.x](https://doi.org/10.1111/j.2153-3490.1964.tb00181.x), 1964.



- 917 Dansgaard, W., and Johnsen, S. J.: A Flow Model and a Time Scale for the Ice Core from Camp
918 Century, Greenland, *Journal of Glaciology*, 8, 215-223, 10.3189/S0022143000031208, 1969.
- 919 Dansgaard, W., Johnsen, S. J., Møller, J., and Langway, C. C.: One Thousand Centuries of Climatic
920 Record from Camp Century on the Greenland Ice Sheet, *Science*, 166, 377-380,
921 10.1126/science.166.3903.377, 1969.
- 922 Dansgaard, W., Johnsen, S. J., Clausen, H. B., Dahl-Jensen, D., Gundestrup, N. S., Hammer, C. U.,
923 Hvidberg, C. S., Steffensen, J. P., Sveinbjörnsdóttir, A. E., Jouzel, J., and Bond, G.: Evidence for
924 general instability of past climate from a 250-kyr ice-core record, *Nature*, 364, 218,
925 10.1038/364218a0, 1993.
- 926 Delmas, R. J., Beer, J., Synal, H.-A., Muscheler, R., Petit, J.-R., and Pourchet, M.: Bomb-test 36Cl
927 measurements in Vostok snow (Antarctica) and the use of 36Cl as a dating tool for deep ice cores,
928 *Tellus B*, 56, 492-498, doi:10.1111/j.1600-0889.2004.00109.x, 2004.
- 929 Denton, G., Alley, R., Comer, G., and Broecker, W.: The role of seasonality in abrupt climate change,
930 *Quaternary Sci Rev*, 24, 1159-1182, 10.1016/j.quascirev.2004.12.002, 2005.
- 931 Durand, N., Deschamps, P., Bard, E., Hamelin, B., Camoin, G., Thomas, A. L., Henderson, G. M.,
932 Yokoyama, Y., and Matsuzaki, H.: Comparison of 14C and U-Th Ages in Corals from IODP #310 Cores
933 Offshore Tahiti, *Radiocarbon*, 55, 1947-1974, 10.2458/azu_js_rc.v55i2.16134, 2013.
- 934 Dykoski, C. A., Edwards, R. L., Cheng, H., Yuan, D., Cai, Y., Zhang, M., Lin, Y., Qing, J., An, Z., and
935 Revenaugh, J.: A high-resolution, absolute-dated Holocene and deglacial Asian monsoon record from
936 Dongge Cave, China, *Earth Planet Sc Lett*, 233, 71-86, <https://doi.org/10.1016/j.epsl.2005.01.036>,
937 2005.
- 938 Edwards, L. R., CHEN, J. H., Ku, T.-L., and Wasserburg, G. J.: Precise Timing of the Last Interglacial
939 Period from Mass Spectrometric Determination of Thorium-230 in Corals, *Science*, 236, 1547-1553,
940 10.1126/science.236.4808.1547, 1987.
- 941 Efron, B.: Bootstrap methods: another look at the jackknife, *The annals of Statistics*, 1-26, 1979.
- 942 Eggleston, S., Schmitt, J., Bereiter, B., Schneider, R., and Fischer, H.: Evolution of the stable carbon
943 isotope composition of atmospheric CO₂ over the last glacial cycle, *Paleoceanography*, 31, 434-452,
944 10.1002/2015PA002874, 2016.
- 945 Fairbanks, R. G., Mortlock, R. A., Chiu, T.-C., Cao, L., Kaplan, A., Guilderson, T. P., Fairbanks, T. W.,
946 Bloom, A. L., Grootes, P. M., and Nadeau, M.-J.: Radiocarbon calibration curve spanning 0 to 50,000
947 years BP based on paired 230Th/234U/238U and 14C dates on pristine corals, *Quaternary Sci Rev*,
948 24, 1781-1796, 10.1016/j.quascirev.2005.04.007, 2005.
- 949 Fedele, F. G., Giaccio, B., Isaia, R., Orsi, G., Carroll, M., and Scaillet, B.: The Campanian Ignimbrite
950 factor: towards a reappraisal of the Middle to Upper Palaeolithic 'transition', *Living under the
951 shadow: cultural impacts of volcanic eruptions*, 19-41, 2007.



- 952 Field, C. V., Schmidt, G. A., Koch, D., and Salyk, C.: Modeling production and climate-related impacts
953 on ^{10}Be concentration in ice cores, *J Geophys Res*, 111, D15107, [10.1029/2005jd006410](https://doi.org/10.1029/2005jd006410), 2006.
- 954 Finkel, R. C., and Nishiizumi, K.: Beryllium 10 concentrations in the Greenland Ice Sheet Project 2 ice
955 core from 3–40 ka, *J Geophys Res*, 102, 26699, [10.1029/97jc01282](https://doi.org/10.1029/97jc01282), 1997.
- 956 Fleitmann, D., Cheng, H., Badertscher, S., Edwards, R. L., Mudelsee, M., Göktürk, O. M., Fankhauser,
957 A., Pickering, R., Raible, C. C., Matter, A., Kramers, J., and Tüysüz, O.: Timing and climatic impact of
958 Greenland interstadials recorded in stalagmites from northern Turkey, *Geophys Res Lett*, 36, L19707,
959 [10.1029/2009GL040050](https://doi.org/10.1029/2009GL040050), 2009.
- 960 Fohlmeister, J., Kromer, B., and Mangini, A.: The Influence of Soil Organic Matter Age Spectrum on
961 the Reconstruction of Atmospheric ^{14}C Levels Via Stalagmites, *Radiocarbon*, 53, 99-115,
962 [10.1017/S003382220003438X](https://doi.org/10.1017/S003382220003438X), 2011.
- 963 Genty, D., and Massault, M.: Carbon transfer dynamics from bomb- ^{14}C and $\delta^{13}\text{C}$ time series of a
964 laminated stalagmite from SW France—modelling and comparison with other stalagmite records,
965 *Geochimica et Cosmochimica Acta*, 63, 1537-1548, [https://doi.org/10.1016/S0016-7037\(99\)00122-2](https://doi.org/10.1016/S0016-7037(99)00122-2),
966 1999.
- 967 Genty, D., Baker, A., Massault, M., Proctor, C., Gilmour, M., Pons-Branchu, E., and Hamelin, B.: Dead
968 carbon in stalagmites: carbonate bedrock paleodissolution vs. ageing of soil organic matter.
969 Implications for ^{13}C variations in speleothems, *Geochimica et Cosmochimica Acta*, 65, 3443-3457,
970 [https://doi.org/10.1016/S0016-7037\(01\)00697-4](https://doi.org/10.1016/S0016-7037(01)00697-4), 2001.
- 971 Giaccio, B., Hajdas, I., Isaia, R., Deino, A., and Nomade, S.: High-precision ^{14}C and $^{40}\text{Ar}/^{39}\text{Ar}$ dating
972 of the Campanian Ignimbrite (Y-5) reconciles the time-scales of climatic-cultural processes at 40 ka,
973 *Scientific Reports*, 7, 45940, [10.1038/srep45940](https://doi.org/10.1038/srep45940)
974 <https://www.nature.com/articles/srep45940#supplementary-information>, 2017.
- 975 Gkinis, V., Simonsen, S. B., Buchardt, S. L., White, J. W. C., and Vinther, B. M.: Water isotope diffusion
976 rates from the NorthGRIP ice core for the last 16,000 years – Glaciological and paleoclimatic
977 implications, *Eart Planet Sc Lett*, 405, 132-141, [http://dx.doi.org/10.1016/j.epsl.2014.08.022](https://doi.org/10.1016/j.epsl.2014.08.022), 2014.
- 978 Guillevic, M., Bazin, L., Landais, A., Kindler, P., Orsi, A., Masson-Delmotte, V., Blunier, T., Buchardt, S.
979 L., Capron, E., Leuenberger, M., Martinerie, P., Prié, F., and Vinther, B. M.: Spatial gradients of
980 temperature, accumulation and $\delta^{18}\text{O}$ -ice in Greenland over a series of Dansgaard-Oeschger
981 events, *Clim. Past*, 9, 1029-1051, [10.5194/cp-9-1029-2013](https://doi.org/10.5194/cp-9-1029-2013), 2013.
- 982 He, F.: Simulating transient climate evolution of the last deglaciation with CCSM 3, PhD, Atmospheric
983 and Ocean Sciences, University of Wisconsin-Madison, 185 pp., 2011.
- 984 Heikkilä, U., Beer, J., and Feichter, J.: Meridional transport and deposition of atmospheric ^{10}Be ,
985 *Atmospheric Chemistry and Physics*, 9, 515-527, [10.5194/acp-9-515-2009](https://doi.org/10.5194/acp-9-515-2009), 2009a.
- 986 Heikkilä, U., Beer, J., Feichter, J., Alfimov, V., Synal, H. A., Schotterer, U., Eichler, A., Schwikowski, M.,
987 and Thompson, L.: ^{36}Cl bomb peak: comparison of modeled and measured data, *Atmos. Chem.*
988 *Phys.*, 9, 4145-4156, [10.5194/acp-9-4145-2009](https://doi.org/10.5194/acp-9-4145-2009), 2009b.



- 989 Heikkilä, U., Beer, J., Abreu, J. A., and Steinhilber, F.: On the Atmospheric Transport and Deposition
990 of the Cosmogenic Radionuclides (10Be): A Review, *Space Science Reviews*, 176, 321-332,
991 10.1007/s11214-011-9838-0, 2011.
- 992 Heikkilä, U., and Smith, A. M.: Production rate and climate influences on the variability of 10Be
993 deposition simulated by ECHAM5-HAM: Globally, in Greenland, and in Antarctica, *J Geophys Res-
994 Atmos*, 118, 2506-2520, 10.1002/jgrd.50217, 2013.
- 995 Henry, L. G., McManus, J. F., Curry, W. B., Roberts, N. L., Piotrowski, A. M., and Keigwin, L. D.: North
996 Atlantic ocean circulation and abrupt climate change during the last glaciation, *Science*, 353, 470-
997 474, 10.1126/science.aaf5529, 2016.
- 998 Herbst, K., Muscheler, R., and Heber, B.: The new local interstellar spectra and their influence on the
999 production rates of the cosmogenic radionuclides 10Be and 14C, *J Geophys Res*, n/a-n/a,
1000 10.1002/2016JA023207, 2016.
- 1001 Hoffmann, D. L., Beck, J. W., Richards, D. A., Smart, P. L., Singarayer, J. S., Ketchmark, T., and
1002 Hawkesworth, C. J.: Towards radiocarbon calibration beyond 28ka using speleothems from the
1003 Bahamas, *Eart Planet Sc Lett*, 289, 1-10, 10.1016/j.epsl.2009.10.004, 2010.
- 1004 Hogg, A., Southon, J., Turney, C., Palmer, J., Ramsey, C. B., Fenwick, P., Boswijk, G., Büntgen, U.,
1005 Friedrich, M., Helle, G., Hughen, K., Jones, R., Kromer, B., Noronha, A., Reinig, F., Reynard, L., Staff,
1006 R., and Wacker, L.: Decadally Resolved Lateglacial Radiocarbon Evidence from New Zealand Kauri,
1007 *Radiocarbon*, 58, 709-733, 10.1017/RDC.2016.86, 2016.
- 1008 Hughen, K., Southon, J., Lehman, S., Bertrand, C., and Turnbull, J.: Marine-derived 14C calibration
1009 and activity record for the past 50,000 years updated from the Cariaco Basin, *Quaternary Sci Rev*, 25,
1010 3216-3227, 10.1016/j.quascirev.2006.03.014, 2006.
- 1011 Johnsen, S. J., Dahl-Jensen, D., Dansgaard, W., and Gundestrup, N.: Greenland palaeotemperatures
1012 derived from GRIP bore hole temperature and ice core isotope profiles, *Tellus B*, 47, 624-629,
1013 10.1034/j.1600-0889.47.issue5.9.x, 1995.
- 1014 Johnsen, S. J., Dahl-Jensen, D., Gundestrup, N., Steffensen, J. P., Clausen, H. B., Miller, H., Masson-
1015 Delmotte, V., Sveinbjörnsdóttir, A. E., and White, J.: Oxygen isotope and palaeotemperature records
1016 from six Greenland ice-core stations: Camp Century, Dye-3, GRIP, GISP2, Renland and NorthGRIP,
1017 *Journal of Quaternary Science*, 16, 299-307, 10.1002/jqs.622, 2001.
- 1018 Kanner, L. C., Burns, S. J., Cheng, H., and Edwards, R. L.: High-Latitude Forcing of the South American
1019 Summer Monsoon During the Last Glacial, *Science*, 335, 570-573, 10.1126/science.1213397, 2012.
- 1020 Köhler, P., Muscheler, R., and Fischer, H.: A model-based interpretation of low-frequency changes in
1021 the carbon cycle during the last 120,000 years and its implications for the reconstruction of
1022 atmospheric $\Delta^{14}\text{C}$, *Geochemistry, Geophysics, Geosystems*, 7, Q11N06, 10.1029/2005GC001228,
1023 2006.



- 1024 Laj, C., Kissel, C., Mazaud, A., Channell, J. E. T., and Beer, J.: North Atlantic palaeointensity stack since
1025 75ka (NAPIS-75) and the duration of the Laschamp event, *Philos T Roy Soc A*, 358, 1009-1025,
1026 10.1098/rsta.2000.0571, 2000.
- 1027 Laj, C., Kissel, C., and Beer, J.: High Resolution Global Paleointensity Stack Since 75 kyr (GLOPIS-75)
1028 Calibrated to Absolute Values, in: *Timescales Of The Paleomagnetic Field*, American Geophysical
1029 Union, 255-265, 2004.
- 1030 Laj, C., Guillou, H., and Kissel, C.: Dynamics of the earth magnetic field in the 10–75 kyr period
1031 comprising the Laschamp and Mono Lake excursions: New results from the French Chaîne des Puy
1032 in a global perspective, *Eart Planet Sc Lett*, 387, 184-197,
1033 <https://doi.org/10.1016/j.epsl.2013.11.031>, 2014.
- 1034 Lal, D., and Peters, B.: Cosmic Ray Produced Radioactivity on the Earth, in: *Kosmische Strahlung II /*
1035 *Cosmic Rays II*, edited by: Sitte, K., *Handbuch der Physik / Encyclopedia of Physics*, Springer Berlin
1036 Heidelberg, Berlin Heidelberg, Germany, 551-612, 1967.
- 1037 Lane, C. S., Brauer, A., Blockley, S. P. E., and Dulski, P.: Volcanic ash reveals time-transgressive abrupt
1038 climate change during the Younger Dryas, *Geology*, 41, 1251-1254, 10.1130/g34867.1, 2013.
- 1039 Lascu, I., Feinberg, J. M., Dorale, J. A., Cheng, H., and Edwards, R. L.: Age of the Laschamp excursion
1040 determined by U-Th dating of a speleothem geomagnetic record from North America, *Geology*, 44,
1041 139-142, 10.1130/g37490.1, 2016.
- 1042 Li, T.-Y., Han, L.-Y., Cheng, H., Edwards, R. L., Shen, C.-C., Li, H.-C., Li, J.-Y., Huang, C.-X., Zhang, T.-T.,
1043 and Zhao, X.: Evolution of the Asian summer monsoon during Dansgaard/Oeschger events 13–17
1044 recorded in a stalagmite constrained by high-precision chronology from southwest China,
1045 *Quaternary Res*, 88, 121-128, 10.1017/qua.2017.22, 2017.
- 1046 Lougheed, B. C., Filipsson, H. L., and Snowball, I.: Large spatial variations in coastal 14C reservoir age
1047 – a case study from the Baltic Sea, *Clim. Past*, 9, 1015-1028, 10.5194/cp-9-1015-2013, 2013.
- 1048 Lukaczyk, C. E.: *36Chlor in Grönlandeis*, PhD, ETH Zurich, Zurich, Switzerland, 285 pp., 1994.
- 1049 Markle, B. R., Steig, E. J., Buizert, C., Schoenemann, S. W., Bitz, C. M., Fudge, T. J., Pedro, J. B., Ding,
1050 Q., Jones, T. R., White, J. W. C., and Sowers, T.: Global atmospheric teleconnections during
1051 Dansgaard-Oeschger events, *Nat Geosci*, 10, 36-40, 10.1038/ngeo2848
1052 <http://www.nature.com/ngeo/journal/v10/n1/abs/ngeo2848.html#supplementary-information>,
1053 2016.
- 1054 Masarik, J., and Beer, J.: Simulation of particle fluxes and cosmogenic nuclide production in the
1055 Earth's atmosphere, *J Geophys Res-Atmos*, 104, 12099-12111, Doi 10.1029/1998jd200091, 1999.
- 1056 Masarik, J., and Beer, J.: An updated simulation of particle fluxes and cosmogenic nuclide production
1057 in the Earth's atmosphere, *J Geophys Res*, 114, D11103, 10.1029/2008jd010557, 2009.



- 1058 Merz, N., Raible, C. C., Fischer, H., Varma, V., Prange, M., and Stocker, T. F.: Greenland accumulation
1059 and its connection to the large-scale atmospheric circulation in ERA-Interim and paleoclimate
1060 simulations, *Clim Past*, 9, 2433-2450, 10.5194/cp-9-2433-2013, 2013.
- 1061 Muscheler, R., Beer, J., Wagner, G., Laj, C., Kissel, C., Raisbeck, G. M., Yiou, F., and Kubik, P. W.:
1062 Changes in the carbon cycle during the last deglaciation as indicated by the comparison of 10Be and
1063 14C records, *Eart Planet Sc Lett*, 219, 325-340, 10.1016/s0012-821x(03)00722-2, 2004.
- 1064 Muscheler, R., Beer, J., Kubik, P. W., and Synal, H. A.: Geomagnetic field intensity during the last
1065 60,000 years based on 10Be and 36Cl from the Summit ice cores and 14C, *Quaternary Sci Rev*, 24,
1066 1849-1860, 10.1016/j.quascirev.2005.01.012, 2005.
- 1067 Muscheler, R., Kromer, B., Björck, S., Svensson, A., Friedrich, M., Kaiser, K. F., and Southon, J.: Tree
1068 rings and ice cores reveal 14C calibration uncertainties during the Younger Dryas, *Nat Geosci*, 1, 263-
1069 267, 10.1038/ngeo128, 2008.
- 1070 Muscheler, R., and Heikkilä, U.: Constraints on long-term changes in solar activity from the range of
1071 variability of cosmogenic radionuclide records, *Astrophysics and Space Sciences Transactions*, 7, 355-
1072 364, 10.5194/astra-7-355-2011, 2011.
- 1073 Muscheler, R., Adolphi, F., and Knudsen, M. F.: Assessing the differences between the IntCal and
1074 Greenland ice-core time scales for the last 14,000 years via the common cosmogenic radionuclide
1075 variations, *Quaternary Sci Rev*, 106, 81-87, 10.1016/j.quascirev.2014.08.017, 2014a.
- 1076 Muscheler, R., Adolphi, F., and Svensson, A.: Challenges in 14C dating towards the limit of the
1077 method inferred from anchoring a floating tree ring radiocarbon chronology to ice core records
1078 around the Laschamp geomagnetic field minimum, *Eart Planet Sc Lett*, 394, 209-215,
1079 10.1016/j.epsl.2014.03.024, 2014b.
- 1080 Nakagawa, T., Kitagawa, H., Yasuda, Y., Tarasov, P. E., Nishida, K., Gotanda, K., and Sawai, Y.:
1081 Asynchronous Climate Changes in the North Atlantic and Japan During the Last Termination, *Science*,
1082 299, 688-691, 10.1126/science.1078235, 2003.
- 1083 Novello, V. F., Cruz, F. W., Vuille, M., Strikis, N. M., Edwards, R. L., Cheng, H., Emerick, S., de Paula,
1084 M. S., Li, X., Barreto, E. d. S., Karmann, I., and Santos, R. V.: A high-resolution history of the South
1085 American Monsoon from Last Glacial Maximum to the Holocene, *Scientific Reports*, 7, 44267,
1086 10.1038/srep44267
1087 <https://www.nature.com/articles/srep44267#supplementary-information>, 2017.
- 1088 Nowaczyk, N. R., Frank, U., Kind, J., and Arz, H. W.: A high-resolution paleointensity stack of the past
1089 14 to 68 ka from Black Sea sediments, *Eart Planet Sc Lett*, 384, 1-16,
1090 <http://dx.doi.org/10.1016/j.epsl.2013.09.028>, 2013.
- 1091 Pedro, J. B., Heikkilä, U. E., Klekociuk, A., Smith, A. M., van Ommen, T. D., and Curran, M. A. J.:
1092 Beryllium-10 transport to Antarctica: Results from seasonally resolved observations and modeling, *J*
1093 *Geophys Res-Atmos*, 116, n/a-n/a, 10.1029/2011jd016530, 2011.



- 1094 Pedro, J. B., McConnell, J. R., van Ommen, T. D., Fink, D., Curran, M. A. J., Smith, A. M., Simon, K. J.,
1095 Moy, A. D., and Das, S. B.: Solar and climate influences on ice core ^{10}Be records from Antarctica and
1096 Greenland during the neutron monitor era, *Eart Planet Sc Lett*, 355-356, 174-186,
1097 10.1016/j.epsl.2012.08.038, 2012.
- 1098 Poluianov, S. V., Kovaltsov, G. A., Mishev, A. L., and Usoskin, I. G.: Production of cosmogenic isotopes
1099 ^7Be , ^{10}Be , ^{14}C , ^{22}Na , and ^{36}Cl in the atmosphere: Altitudinal profiles of yield functions, *J Geophys*
1100 *Res-Atmos*, 121, 8125-8136, 10.1002/2016JD025034, 2016.
- 1101 Raisbeck, G. M., Yiou, F., Fruneau, M., Loiseaux, J. M., Lieuvin, M., and Ravel, J. C.:
1102 Cosmogenic $^{10}\text{Be}/^7\text{Be}$ as a probe of atmospheric transport processes, *Geophys Res Lett*, 8, 1015-
1103 1018, 10.1029/GL008i009p01015, 1981.
- 1104 Raisbeck, G. M., Yiou, F., Jouzel, J., and Stocker, T. F.: Direct north-south synchronization of abrupt
1105 climate change record in ice cores using Beryllium 10, *Clim Past*, 3, 541-547, 10.5194/cp-3-541-2007,
1106 2007.
- 1107 Raisbeck, G. M., Cauquoin, A., Jouzel, J., Landais, A., Petit, J. R., Lipenkov, V. Y., Beer, J., Synal, H. A.,
1108 Oerter, H., Johnsen, S. J., Steffensen, J. P., Svensson, A., and Yiou, F.: An improved north-south
1109 synchronization of ice core records around the 41 kyr ^{10}Be peak, *Clim. Past*, 13, 217-229,
1110 10.5194/cp-13-217-2017, 2017.
- 1111 Rasmussen, S. O., Andersen, K. K., Svensson, A. M., Steffensen, J. P., Vinther, B. M., Clausen, H. B.,
1112 Siggaard-Andersen, M. L., Johnsen, S. J., Larsen, L. B., Dahl-Jensen, D., Bigler, M., Röthlisberger, R.,
1113 Fischer, H., Goto-Azuma, K., Hansson, M. E., and Ruth, U.: A new Greenland ice core chronology for
1114 the last glacial termination, *J Geophys Res*, 111, D06102, 10.1029/2005jd006079, 2006.
- 1115 Rasmussen, S. O., Seierstad, I. K., Andersen, K. K., Bigler, M., Dahl-Jensen, D., and Johnsen, S. J.:
1116 Synchronization of the NGRIP, GRIP, and GISP2 ice cores across MIS 2 and palaeoclimatic
1117 implications, *Quaternary Sci Rev*, 27, 18-28, 10.1016/j.quascirev.2007.01.016, 2008.
- 1118 Rasmussen, S. O., Abbott, P. M., Blunier, T., Bourne, A. J., Brook, E., Buchardt, S. L., Buizert, C.,
1119 Chappellaz, J., Clausen, H. B., Cook, E., Dahl-Jensen, D., Davies, S. M., Guillevic, M., Kipfstuhl, S.,
1120 Laepple, T., Seierstad, I. K., Severinghaus, J. P., Steffensen, J. P., Stowasser, C., Svensson, A.,
1121 Vallenga, P., Vinther, B. M., Wilhelms, F., and Winstrup, M.: A first chronology for the North
1122 Greenland Eemian Ice Drilling (NEEM) ice core, *Clim. Past*, 9, 2713-2730, 10.5194/cp-9-2713-2013,
1123 2013.
- 1124 Rasmussen, S. O., Bigler, M., Blockley, S. P., Blunier, T., Buchardt, S. L., Clausen, H. B., Cvijanovic, I.,
1125 Dahl-Jensen, D., Johnsen, S. J., Fischer, H., Gkinis, V., Guillevic, M., Hoek, W. Z., Lowe, J. J., Pedro, J.
1126 B., Popp, T., Seierstad, I. K., Steffensen, J. P., Svensson, A. M., Vallenga, P., Vinther, B. M., Walker,
1127 M. J. C., Wheatley, J. J., and Winstrup, M.: A stratigraphic framework for abrupt climatic changes
1128 during the Last Glacial period based on three synchronized Greenland ice-core records: refining and
1129 extending the INTIMATE event stratigraphy, *Quaternary Sci Rev*, 106, 14-28,
1130 <http://dx.doi.org/10.1016/j.quascirev.2014.09.007>, 2014a.
- 1131 Rasmussen, S. O., Birks, H. H., Blockley, S. P. E., Brauer, A., Hajdas, I., Hoek, W. Z., Lowe, J. J.,
1132 Moreno, A., Renssen, H., Roche, D. M., Svensson, A. M., Valdes, P., and Walker, M. J. C.: Dating,



- 1133 synthesis, and interpretation of palaeoclimatic records of the Last Glacial cycle and model-data
1134 integration: advances by the INTIMATE (INTEgration of Ice-core, MARine and TERrestrial records)
1135 COST Action ES0907, *Quaternary Sci Rev*, 106, 1-13,
1136 <http://dx.doi.org/10.1016/j.quascirev.2014.10.031>, 2014b.
- 1137 Reimer, P. J., Bard, E., Bayliss, A., Beck, J. W., Blackwell, P. G., Bronk Ramsey, C., Buck, C. E., Cheng,
1138 H., Edwards, R. L., Friedrich, M., Grootes, P. M., Guilderson, T. P., Hafliðason, H., Hajdas, I., Hatté, C.,
1139 Heaton, T. J., Hoffmann, D. L., Hogg, A. G., Hughen, K. A., Kaiser, K. F., Kromer, B., Manning, S. W.,
1140 Niu, M., Reimer, R. W., Richards, D. A., Scott, E. M., Southon, J. R., Staff, R. A., Turney, C. S. M., and
1141 van der Plicht, J.: IntCal13 and Marine13 Radiocarbon Age Calibration Curves 0–50,000 Years cal BP,
1142 *Radiocarbon*, 55, 1869-1887, [10.2458/azu_js_rc.55.16947](https://doi.org/10.2458/azu_js_rc.55.16947), 2013.
- 1143 Roth, R., and Joos, F.: A reconstruction of radiocarbon production and total solar irradiance from the
1144 Holocene 14C and CO2 records: implications of data and model uncertainties, *Clim Past*, 9, 1879-
1145 1909, [10.5194/cp-9-1879-2013](https://doi.org/10.5194/cp-9-1879-2013), 2013.
- 1146 Schüpbach, S., Fischer, H., Bigler, M., Erhardt, T., Gfeller, G., Leuenberger, D., Mini, O., Mulvaney, R.,
1147 Abram, N. J., Fleet, L., Frey, M. M., Thomas, E., Svensson, A., Dahl-Jensen, D., Kettner, E., Kjaer, H.,
1148 Seierstad, I., Steffensen, J. P., Rasmussen, S. O., Vallelonga, P., Winstrup, M., Wegner, A., Twarloh,
1149 B., Wolff, K., Schmidt, K., Goto-Azuma, K., Kuramoto, T., Hirabayashi, M., Uetake, J., Zheng, J.,
1150 Bourgeois, J., Fisher, D., Zhiheng, D., Xiao, C., Legrand, M., Spolaor, A., Gabrieli, J., Barbante, C., Kang,
1151 J. H., Hur, S. D., Hong, S. B., Hwang, H. J., Hong, S., Hansson, M., Iizuka, Y., Oyabu, I., Muscheler, R.,
1152 Adolphi, F., Maselli, O., McConnell, J., and Wolff, E. W.: Greenland records of aerosol source and
1153 atmospheric lifetime changes from the Eemian to the Holocene, *Nat Commun*, 9, 1476,
1154 [10.1038/s41467-018-03924-3](https://doi.org/10.1038/s41467-018-03924-3), 2018.
- 1155 Seierstad, I. K., Abbott, P. M., Bigler, M., Blunier, T., Bourne, A. J., Brook, E., Buchardt, S. L., Buizert,
1156 C., Clausen, H. B., Cook, E., Dahl-Jensen, D., Davies, S. M., Guillevic, M., Johnsen, S. J., Pedersen, D. S.,
1157 Popp, T. J., Rasmussen, S. O., Severinghaus, J. P., Svensson, A., and Vinther, B. M.: Consistently dated
1158 records from the Greenland GRIP, GISP2 and NGRIP ice cores for the past 104 ka reveal regional
1159 millennial-scale $\delta^{18}O$ gradients with possible Heinrich event imprint, *Quaternary Sci Rev*, 106, 29-46,
1160 <http://dx.doi.org/10.1016/j.quascirev.2014.10.032>, 2014.
- 1161 Siegenthaler, U., Heimann, M., and Oeschger, H.: 14C variations caused by changes in the global
1162 carbon cycle, *Radiocarbon*, 22, 177-191, 1980.
- 1163 Singer, B. S., Guillou, H., Jicha, B. R., Laj, C., Kissel, C., Beard, B. L., and Johnson, C. M.: 40Ar/39Ar, K-
1164 Ar and 230Th–238U dating of the Laschamp excursion: A radioisotopic tie-point for ice core and
1165 climate chronologies, *Eart Planet Sc Lett*, 286, 80-88, <http://dx.doi.org/10.1016/j.epsl.2009.06.030>,
1166 2009.
- 1167 Southon, J.: A First Step to Reconciling the GRIP and GISP2 Ice-Core Chronologies, 0–14,500 yr B.P.,
1168 *Quaternary Res*, 57, 32-37, [10.1006/qres.2001.2295](https://doi.org/10.1006/qres.2001.2295), 2002.
- 1169 Southon, J., Noronha, A. L., Cheng, H., Edwards, R. L., and Wang, Y.: A high-resolution record of
1170 atmospheric 14C based on Hulu Cave speleothem H82, *Quaternary Sci Rev*, 33, 32-41,
1171 [10.1016/j.quascirev.2011.11.022](https://doi.org/10.1016/j.quascirev.2011.11.022), 2012.



- 1172 Staff, R. A., Scholout, G., Ramsey, C. B., Brock, F., Bryant, C. L., Kitagawa, H., Van der Plicht, J.,
1173 Marshall, M. H., Brauer, A., and Lamb, H. F.: Integration of the old and new Lake Suigetsu (Japan)
1174 terrestrial radiocarbon calibration data sets, *Radiocarbon*, 55, 2049-2058, 2013.
- 1175 Strikis, N. M., Cruz, F. W., Barreto, E. A. S., Naughton, F., Vuille, M., Cheng, H., Voelker, A. H. L.,
1176 Zhang, H., Karmann, I., Edwards, R. L., Auler, A. S., Santos, R. V., and Sales, H. R.: South American
1177 monsoon response to iceberg discharge in the North Atlantic, *Proceedings of the National Academy*
1178 *of Sciences*, 10.1073/pnas.1717784115, 2018.
- 1179 Stuiver, M., and Polach, H. A.: Discussion; reporting of C-14 data, *Radiocarbon*, 19, 355-363, 1977.
- 1180 Svensson, A., Andersen, K. K., Bigler, M., Clausen, H. B., Dahl-Jensen, D., Davies, S. M., Johnsen, S. J.,
1181 Muscheler, R., Rasmussen, S. O., and Röthlisberger, R.: The Greenland Ice Core Chronology 2005,
1182 15–42ka. Part 2: comparison to other records, *Quaternary Sci Rev*, 25, 3258-3267,
1183 10.1016/j.quascirev.2006.08.003, 2006.
- 1184 Svensson, A., Andersen, K. K., Bigler, M., Clausen, H. B., Dahl-Jensen, D., Davies, S. M., Johnsen, S. J.,
1185 Muscheler, R., Parrenin, F., Rasmussen, S. O., Röthlisberger, R., Seierstad, I., Steffensen, J. P., and
1186 Vinther, B. M.: A 60 000 year Greenland stratigraphic ice core chronology, *Clim Past*, 4, 47-57,
1187 10.5194/cp-4-47-2008, 2008.
- 1188 Thomas, Z. A.: Using natural archives to detect climate and environmental tipping points in the Earth
1189 System, *Quaternary Sci Rev*, 152, 60-71, <https://doi.org/10.1016/j.quascirev.2016.09.026>, 2016.
- 1190 Trumbore, S.: AGE OF SOIL ORGANIC MATTER AND SOIL RESPIRATION: RADIOCARBON CONSTRAINTS
1191 ON BELOWGROUND C DYNAMICS, *Ecological Applications*, 10, 399-411, 10.1890/1051-
1192 0761(2000)010[0399:AOSOMA]2.0.CO;2, 2000.
- 1193 Turney, C. S. M., Thomas, Z. A., Hutchinson, D. K., Bradshaw, C. J. A., Brook, B. W., England, M. H.,
1194 Fogwill, C. J., Jones, R. T., Palmer, J., Hughen, K. A., and Cooper, A.: Obliquity - driven expansion of
1195 North Atlantic sea ice during the last glacial, *Geophys Res Lett*, 42, 10,382-310,390,
1196 doi:10.1002/2015GL066344, 2015.
- 1197 Turney, C. S. M., Palmer, J., Bronk Ramsey, C., Adolphi, F., Muscheler, R., Hughen, K. A., Staff, R. A.,
1198 Jones, R. T., Thomas, Z. A., Fogwill, C. J., and Hogg, A.: High-precision dating and correlation of ice,
1199 marine and terrestrial sequences spanning Heinrich Event 3: Testing mechanisms of
1200 interhemispheric change using New Zealand ancient kauri (*Agathis australis*), *Quaternary Sci Rev*,
1201 137, 126-134, <http://dx.doi.org/10.1016/j.quascirev.2016.02.005>, 2016.
- 1202 Veres, D., Bazin, L., Landais, A., Toyé Mahamadou Kele, H., Lemieux-Dudon, B., Parrenin, F.,
1203 Martinerie, P., Blayo, E., Blunier, T., Capron, E., Chappellaz, J., Rasmussen, S. O., Severi, M.,
1204 Svensson, A., Vinther, B., and Wolff, E. W.: The Antarctic ice core chronology (AICC2012): an
1205 optimized multi-parameter and multi-site dating approach for the last 120 thousand years, *Clim*
1206 *Past*, 9, 1733-1748, 10.5194/cp-9-1733-2013, 2013.
- 1207 Vinther, B. M., Clausen, H. B., Johnsen, S. J., Rasmussen, S. O., Andersen, K. K., Buchardt, S. L., Dahl-
1208 Jensen, D., Seierstad, I. K., Siggaard-Andersen, M. L., Steffensen, J. P., Svensson, A., Olsen, J., and



- 1209 Heinemeier, J.: A synchronized dating of three Greenland ice cores throughout the Holocene, *J*
1210 *Geophys Res*, 111, D13102, [10.1029/2005jd006921](https://doi.org/10.1029/2005jd006921), 2006.
- 1211 Vogt, S., Herzog, G. F., and Reedy, R. C.: Cosmogenic nuclides in extraterrestrial materials, *Rev*
1212 *Geophys*, 28, 253-275, [10.1029/RG028i003p00253](https://doi.org/10.1029/RG028i003p00253), 1990.
- 1213 Wagner, G., Masarik, J., Beer, J., Baumgartner, S., Imboden, D., Kubik, P. W., Synal, H. A., and Suter,
1214 M.: Reconstruction of the geomagnetic field between 20 and 60 kyr BP from cosmogenic
1215 radionuclides in the GRIP ice core, *Nuclear Instruments and Methods in Physics Research Section B:*
1216 *Beam Interactions with Materials and Atoms*, 172, 597-604, [https://doi.org/10.1016/S0168-](https://doi.org/10.1016/S0168-583X(00)00285-8)
1217 [583X\(00\)00285-8](https://doi.org/10.1016/S0168-583X(00)00285-8), 2000.
- 1218 Wagner, G., Beer, J., Masarik, J., Muscheler, R., Kubik, P. W., Mende, W., Laj, C., Raisbeck, G. M., and
1219 Yiou, F.: Presence of the Solar de Vries Cycle (~205 years) during the Last Ice Age, *Geophys Res Lett*,
1220 28, 303-306, [10.1029/2000gl006116](https://doi.org/10.1029/2000gl006116), 2001a.
- 1221 Wagner, G., Laj, C., Beer, J., Kissel, C., Muscheler, R., Masarik, J., and Synal, H. A.: Reconstruction of
1222 the paleoaccumulation rate of central Greenland during the last 75 kyr using the cosmogenic
1223 radionuclides ^{36}Cl and ^{10}Be and geomagnetic field intensity data, *Eart Planet Sc Lett*, 193, 515-521,
1224 [10.1016/s0012-821x\(01\)00504-0](https://doi.org/10.1016/s0012-821x(01)00504-0), 2001b.
- 1225 Wang, Y. J., Cheng, H., Edwards, R. L., An, Z. S., Wu, J. Y., Shen, C. C., and Dorale, J. A.: A high-
1226 resolution absolute-dated late Pleistocene Monsoon record from Hulu Cave, China, *Science*, 294,
1227 2345-2348, [10.1126/science.1064618](https://doi.org/10.1126/science.1064618), 2001.
- 1228 Watson, L. R., Van Doren, J. M., Davidovits, P., Worsnop, D. R., Zahniser, M. S., and Kolb, C. E.:
1229 Uptake of HCl molecules by aqueous sulfuric acid droplets as a function of acid concentration, *J*
1230 *Geophys Res-Atmos*, 95, 5631-5638, [doi:10.1029/JD095iD05p05631](https://doi.org/10.1029/JD095iD05p05631), 1990.
- 1231 Werner, M., Mikolajewicz, U., Heimann, M., and Hoffmann, G.: Borehole versus isotope
1232 temperatures on Greenland: Seasonality does matter, *Geophys Res Lett*, 27, 723-726,
1233 [10.1029/1999gl006075](https://doi.org/10.1029/1999gl006075), 2000.
- 1234 Werner, M., Heimann, M., and Hoffmann, G.: Isotopic composition and origin of polar precipitation
1235 in present and glacial climate simulations, *Tellus B*, 53, 53-71, [10.1034/j.1600-0889.2001.01154.x](https://doi.org/10.1034/j.1600-0889.2001.01154.x),
1236 2001.
- 1237 Yiou, F., Raisbeck, G. M., Baumgartner, S., Beer, J., Hammer, C., Johnsen, S., Jouzel, J., Kubik, P. W.,
1238 Lestringuez, J., Stievenard, M., Suter, M., and Yiou, P.: Beryllium 10 in the Greenland Ice Core Project
1239 ice core at Summit, Greenland, *J Geophys Res*, 102, 26783, [10.1029/97jc01265](https://doi.org/10.1029/97jc01265), 1997.
- 1240 Zerle, L., Faestermann, T., Knie, K., Korschinek, G., Nolte, E., Beer, J., and Schotterer, U.: The ^{41}Ca
1241 bomb pulse and atmospheric transport of radionuclides, *J Geophys Res-Atmos*, 102, 19517-19527,
1242 [10.1029/97JD00701](https://doi.org/10.1029/97JD00701), 1997.
1243